JMB

Available online at www.sciencedirect.com

ScienceDirect

ELSEVIER

Directed Evolution of an Anti-prion Protein scFv Fragment to an Affinity of 1 pM and its Structural Interpretation

Béatrice Luginbühl[1], Zoltan Kanyo[2], R. Mark Jones[3] Robert J. Fletterick[2], Stanley B. Prusiner[2,4,5], Fred E. Cohen[2,4] R. Anthony Williamson[6], Dennis R. Burton[6] and Andreas Plückthun[1]*

[1]*Biochemisches Institut Universität Zürich Winterthurerstrasse 190 CH-8057 Zürich, Switzerland*

[2]*Department of Biochemistry and Biophysics, University of California, San Francisco, CA 94143, USA*

[3]*Sapidyne Instruments Inc., 967 East Park Center Boulevard 445 Boise, Idaho 83706, USA*

[4]*Institute for Neurodegenerative Diseases, University of California, San Francisco, CA 94143, USA*

[5]*Department of Neurology, University of California, San Francisco, CA 94143, USA*

[6]*Department of Immunology The Scripps Research Institute La Jolla, CA 92037, USA*

*Corresponding author

Bovine spongiform encephalopathy (BSE) is a fatal neurodegenerative prion disease affecting cattle that is transmissible to humans, manifesting as a variant of Creutzfeldt-Jakob disease (vCJD) likely following the consumption of meat contaminated with BSE prions. High-affinity antibodies are a prerequisite for the development of simple, highly sensitive and non-invasive diagnostic tests that are able to detect even small amounts of the disease-associated PrP conformer (PrP^{Sc}). We describe here the affinity maturation of a single-chain Fv antibody fragment with a binding affinity of 1 pM to a peptide derived from the unstructured region of bovine PrP (BoPrP (90–105)). This is the tightest peptide-binding antibody reported to date and may find useful application in diagnostics, especially when PrP^{Sc} is pretreated by denaturation and/or proteolysis for peptide-like presentation. Several rounds of directed evolution and off-rate selection with ribosome display were performed using an antibody library generated from a single PrP binder with error-prone PCR and DNA-shuffling. As the correct determinations of affinities in this range are not straightforward, competition biosensor techniques and KinExA methods were both applied and compared. Structural interpretation of the affinity improvement was performed based on the crystal structure of the original prion binder in complex with the BoPrP (95–104) peptide by modeling the corresponding mutations.

© 2006 Elsevier Ltd. All rights reserved.

Keywords: prion; antibody engineering; crystal structure; Biacore; KinExA

Introduction

Prion diseases, also known as transmissible spongiform encephalopathies (TSEs), are a group of fatal neurodegenerative disorders characterized by neural cell loss, spongiform change of the brain (vacuolation), astrogliosis and the accumulation of an abnormal isoform of the prion protein (PrP^{Sc}) in the nervous system. In humans and animals, several TSEs are known, including Creutzfeldt-Jakob disease (CJD), Gerstmann-Sträussler-Scheinker syndrome (GSS), fatal familial insomnia (FFI) and kuru in humans, scrapie in sheep (from which the abbreviation Sc in PrP^{Sc} originally derives), chronic wasting disease (CWD) in deer and elk and bovine spongiform encephalopathy (BSE) in cattle.[1–3]

An essential component of the disease-causing agent is the pathological isoform (PrP^{Sc}) of the normal cellular prion protein (PrP^C), which is a GPI-anchored membrane glycoprotein present in the brain, as well as being constitutively expressed in many cell types.[4,5] The conversion of PrP^C to PrP^{Sc} involves a conformational change in which the α-helical content of PrP^C is reduced whilst the amount of β-sheet dramatically increases.[6] These structural alterations seem to promote aggregation of the protein, characterized by low solubility and protease resistance (PrP 27–30).

Upon more detailed investigations of prion diseases, specific antibodies became of interest, e.g. for structural characterization,[7,8] investigation of amyloid fibril formation,[9] as well as for new opportunities in diagnostics[10,11] and even as potential therapeutic agents.[12,13] The use of PrP knockout mice (Prnp$^{0/0}$) is necessary to elicit the production of PrP-specific antibodies.[14] The application of combinatorial antibody libraries in combination with *in vitro* selection technologies such as ribosome display,[15] mRNA display[16] and phage display[17] offers a powerful approach to isolate and affinity-mature PrP-specific antibodies.

The compelling experimental evidence linking the new variant of CJD (vCJD) in humans with the consumption of meat contaminated with the BSE agent[18] have raised severe concerns about possible epidemic propagation throughout the human population. The prevention of exposure of humans to BSE-contaminated meat and animal products and the horizontal spread of vCJD within the human population *via* iatrogenic transmission including blood transfusion[19] is of major importance and reinforces the need for highly sensitive diagnostics of prion infection and contamination. The use of directed *in vitro* evolution methods together with combinatorial antibody libraries facilitates the selection of high-affinity PrP-specific antibodies and may pave the way to new highly sensitive assays.

Here, we describe such an example of successful *in vitro* affinity maturation of an ultra-high affinity antibody that recognizes a peptide from the unstructured region of bovine PrP (BoPrP (90–105)), using directed molecular evolution and ribosome display. Starting from the previously described P Fab,[20] we generated a library with DNA-shuffling and error-prone PCR using dNTP analogs. With repeating cycles of off-rate selection and randomization, the scFv fragment termed C1 with a K_D of 1 pM for BoPrP (90–105) could be selected. Solution-based affinity determination methods (competition Biacore and the Kinetic Exclusion Assay (KinExA)) were performed to measure accurately a system with such a high affinity. The advantages and limitations of both methods for measurements in the low picomolar affinity range are discussed. A 13-fold affinity improvement of the selected clone C1, compared to the progenitor P scFv, against BoPrP (90–105) was determined. A structural interpretation of the affinity improvement was carried out, based on the crystal structure of the original Fab fragment of antibody P in complex with the BoPrP (95–104) peptide. Modeling the mutations of the antibody C1 in the structure of the complex revealed additional ionic and hydrophobic interactions with the peptide, most probably responsible for the affinity improvement.

With this ultra-high affinity anti-PrP peptide antibody C1, we have a diagnostic tool at hand, which may be applicable in a wide variety of immunoassays for BSE detection, provided the PrP is presented in a peptide-like conformation. This can be achieved by denaturation, especially when preceded by a partial proteolytic digest of the protein, as is commonly done in prion diagnostics.[21,20] The C1 antibody may prove to be an excellent tool to meet the increased demand of highly sensitive diagnostic BSE tests for the detection of small amounts of PrP^{Sc} present in brain tissue or other peripheral tissues. Furthermore, it is a generally useful model system to study the extremely tight binding of peptides.

Results

Origin of P Fab and antibody format conversion

P Fab was originally selected by phage display from a mouse IgG1 κ Fab library, which had been prepared from bone marrow, spleen and lymph tissue of a Prnp$^{0/0}$ mouse, immunized with the synthetic peptide BoPrP (96–115).[20] The phage selection had been performed with immobilized recombinant bovine PrP 23–231 (BoPrP (23–231)) protein and with immobilized recombinant mouse/bovine chimeric construct MBo2Mo (composed of mouse residues 23–231, except for residues 90–144, which are bovine). Epitope mapping of P Fab fragment revealed a linear epitope comprising residues 96–104. This epitope was directly confirmed with the crystal structure of the complex of P Fab fragment and peptide (as described in this paper). Expression of the antibody P as a chimeric human–mouse Fab (chFab, muV$_L$κ–huC$_L$κ, muV$_H$–huC$_H$γ1) and subsequent affinity determination with kinetic

Biacore at 25 °C resulted in K_D values of 0.5 nM and 0.3 nM, measured with immobilized BoPrP (90–145) and MBo2Mo (23–231) protein, respectively.[20]

We wished to improve the affinity of antibody P. Since one of the most powerful ways to achieve this is to combine directed molecular evolution with ribosome display, the two unlinked variable domains in the Fab fragment had to be converted to the single-chain Fv fragment (scFv) format. The two variable domains V_L and V_H were thus linked in the orientation V_L-V_H by a 19 amino acid linker encoding the sequence PNGASNSSSAPETSSASGS.[22]

Library construction

Random mutagenesis and DNA-shuffling were combined in generating two libraries based on the P scFv fragment. Library 1 (Figure 1), with low mutational load, was generated by Taq polymerase amplification and DNA-shuffling, mimicking

homologous recombination *in vitro*.[23] Library 2, with high mutational load, was created by error-prone amplification of P scFv fragment with nucleotide analogs and, in a second step, subjected to DNA-shuffling, thus allowing combinatorial recombination of the mutations generated. The nucleotide analogs dPTP and 8-oxo-GTP introduce both transversion and transition mutations without insertions or deletions. As shown previously,[24,25] the mutation frequency can be modulated both by the number of PCR cycles and by the concentration of nucleotide analogs used.

For library 2, 18 cycles of DNA amplification in the presence of a fourfold molar excess of normal dNTPs to dNTP analogs were used. The mutation rate for library 2 was determined as 28 kb^{-1}, which resulted in an average of 11.3 amino acid changes per gene, whereas library 1 exhibited a mutation rate of 12 kb^{-1}, corresponding to an average mutational load of 4.8 amino acid changes per gene. Library 1
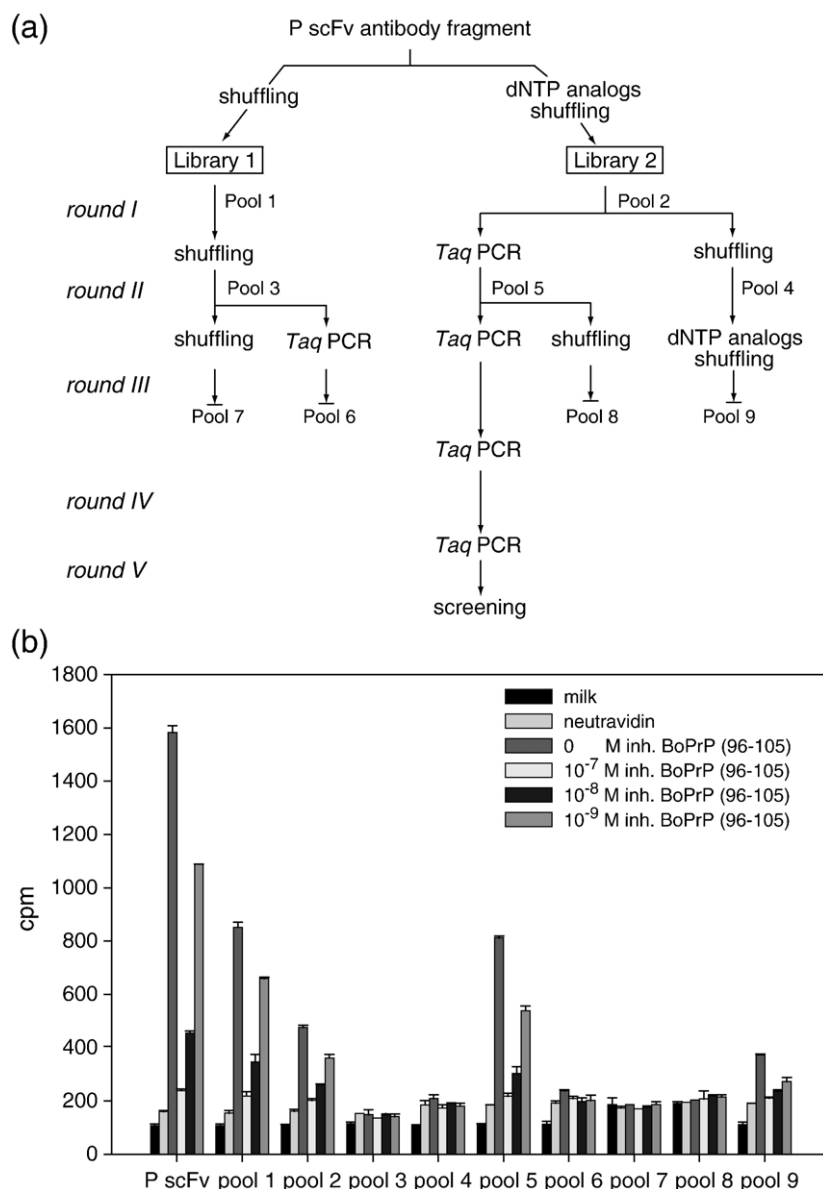

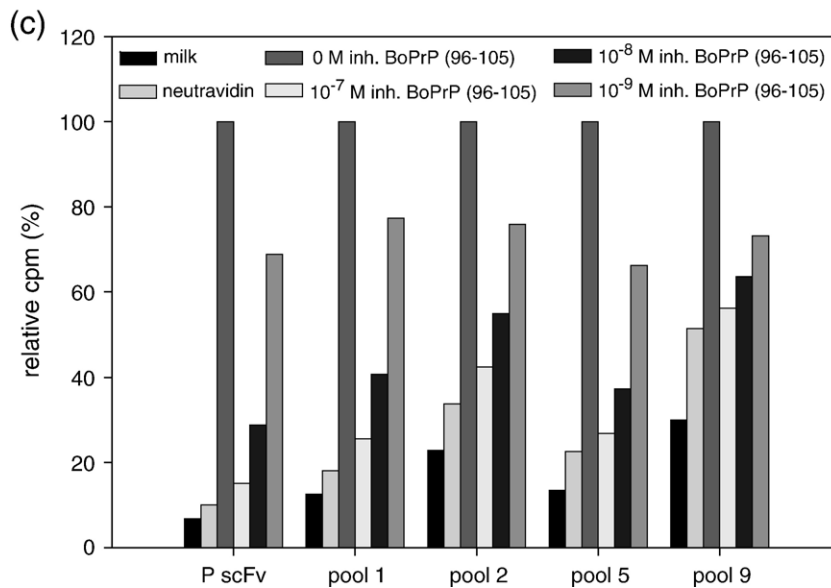
Figure 1 (*legend on next page*)

Figure 1. Scheme of directed evolution with ribosome display using off-rate selection and inhibition RIA of pools from round I to III. (a) Starting with the P scFv fragment, two libraries with low and a high mutation rate were generated. The low mutation rate (12 mutations kb^{-1}) library 1 was created by DNA-shuffling and Taq polymerase amplification, whereas the high mutation rate (28 mutations kb^{-1}) library 2 was obtained by error-prone amplification with nucleotide analogs (dPTP and 8-oxo-GTP) and DNA-shuffling. In total, five rounds of off-rate selection with competing unlabeled BoPrP (90–105) peptide with exposure times from 12 h to ten days were performed with library 2, with no further diversification steps between the rounds, except those occurring by errors inherent in Taq polymerase amplification. Pools 3, 4, 6, 7, 8, 9, which were exposed to alternating DNA-shuffling and error-prone PCR with nucleotide analogs, were not further investigated after the third round due to low mean activity in the inhibition RIA (see Figure 1(b)). (b) The scFv proteins present in the different pools after the third round were radioactively labeled by *in vitro* expression in the presence of [^{35}S]Met. The ^{35}S-labeled proteins were equilibrated with 0 M to 10^{-9} M of competitor peptide BoPrP (96–105) and subsequently subjected to surface-immobilized antigen and control surfaces (milk, neutravidin). The uninhibited binding signal is a measure of the mean activity of the pool (percentage of antibodies with binding activity), whereas the inhibited signal represents the amount of uncomplexed scFv at equilibrium able to bind to the ELISA plate. Higher affinity antibodies will already be competed by low concentrations of soluble antigen from binding to the ELISA plate. The uninhibited binding signal of pools 3, 4, 6, 7, and 8 reached only background level, and thus essentially no binding activity is retained in these pools. Pools 1, 2, 5 and 9 retained binding activities of 54 %, 30 %, 51 % and 23 %, respectively, with respect to the P scFv. The signal increase of pool 5 by 21 % compared to the predecessor pool 2 indicates the enrichment of active scFv proteins throughout round II. (c) Since the relative inhibition signals were not significantly "improved" (did not become lower) in the active pools, additional rounds with Taq PCR were performed with pool 5 to increase the affinity further.

and library 2 were subsequently subjected to several rounds of off-rate selection with ribosome display.

Affinity evolution with off-rate selection

Two strategies are possible to improve the affinity of the antibody P with directed molecular evolution in combination with ribosome display. First, the selection of affinity-improved binders can be achieved under conditions of limiting amounts of PrP peptide,[26] where at equilibrium, the immobilized peptide should be mainly bound by the tightest affinity molecules. When using this strategy, it has to be considered, however, that few high affinity antibodies displayed on the ribosome may be competed out by many lesser affinity (parent) antibodies. By choosing the antigen concentration below the desired K_D value, but still above the antibody concentration, a binding-driven selection pressure can be generated which favors higher affinity binders,[27] but the strategy becomes more difficult the smaller the K_D becomes. A

second strategy focuses on the kinetics of dissociation from the prion peptide. The dissociation rate constant (k_{off}) can be improved by exposing the library to an excess of competitor during the ribosome display round. In this case, the selection pressure can be adjusted by increasing the time that the ribosomal complexes are exposed to the competitor.[28]

In previous studies, it was found that in ribosome display the most efficient selection strategy for affinity maturation was off-rate selection.[29] Furthermore, the association rate constant (k_{on}) is limited by diffusion and the geometric constraints of the binding sites, including the desolvation of the binding interface,[30,31] and thus affinity improvements usually are caused by slower dissociation rates. The high salt conditions during the ribosome display selection round can make the selection for faster k_{on} difficult, as they would screen electrostatic effects, which are thought to be important for causing faster on-rates, but they would only be effective at low salt concentrations anyway.[32]

In addition to the binding interaction, the stability of the immobilized target protein might be affected by the high Mg^{2+} and K^+ concentrations in ribosome display.[33] This is true especially for off-rate selection, where long competitive incubation is the key element in the experimental set-up, only very stable and non-aggregation-prone target proteins (antigens) can be used. Due to the high aggregation propensies of BoPrP (90–145) and the MBo2Mo protein in high salt and at neutral pH (data not shown), these proteins could not be used as antigen for selection with ribosome display. Instead, a 16-mer peptide, BoPrP (90–105) comprising the epitope and a natural spacer sequence at the N terminus, required for sufficient epitope accessibility upon surface immobilization, was successfully applied as immobilized target during the selection. The change from a long peptide antigen with potential structure and aggregation propensity to a short peptide antigen that does not seem to aggregate improved the measured affinity of the P chFab fragment 30-fold from 0.5 nM[20] for the BoPrP (90–145) protein to 18 pM for the BoPrP (90–105) peptide (Table 1). This suggests that the short peptide spends a greater fraction of its time in a binding-competent conformation, whereas the long peptide may be in equilibrium with one or more binding-incompetent conformations. We decided to affinity-mature the P Fab further by off-rate selection, trying to achieve even lower affinities than 18 pM for the antibody P binding its peptide antigen. Affinity maturation toward the low picomolar range has been accomplished before,[29,34,35] and we wished to extend the limits for peptide binders even further.

Prior to the off-rate selection experiments, the two initial libraries (1 and 2) generated from the P scFv fragment were changed into the ribosome display format by inserting them into the vector pRDVgeneIII (see Materials and Methods). Thereby, a

protein spacer derived from gene III of filamentous phage M13 was fused to the C terminus of the scFvs, allowing functional display of the antibody on the ribosome.[36]

After *in vitro* translation of the libraries, the ribosomal complexes were equilibrated with biotinylated BoPrP (90–105) peptide. A 1000-fold excess of free, non-biotinylated antigen BoPrP (90–105) was then added to the reaction mixture. Ribosomal complexes with fast off-rates that dissociate from the biotinylated antigen will be captured by the free antigen. By increasing the exposure time to the competitor from round to round, only those ribosomal complexes with slower off-rates remain bound to the biotinylated antigen and are rescued by the streptavidin-coated magnetic beads. In the random mutagenesis procedure, many molecules are produced that are totally non-functional, or even carry stop codons before selection. Therefore, an additional non-stringent enrichment round after the off-rate selection step was performed to reduce the background level of nonspecific complexes and any mRNA that might be directly sticking to the streptavidin-coated magnetic beads.

In a total of five rounds of ribosome display, off-rate selection with increasing competitor exposure time from 12 h up to ten days was performed (Figure 1(a)). Library 1 was subjected to DNA-shuffling after each round (pool 3 and 7), except for pool 6, which was only Taq amplified. After the first round, the pool of library 2 was split into two pools (4 and 5). Pool 4 was alternately subjected to DNA-shuffling and error-prone randomization with dNTP analogs in combination with DNA-shuffling. Pool 5 was only amplified with Taq polymerase (Figure 1(a)).

After three rounds of off-rate selection (80 h competitor incubation), the binding activity and antigen specificity of the different pools were examined with inhibition RIA (Figure 1(b)). After *in vitro* translation of the different pools in the presence of $[^{35}S]$Met, the radioactively labeled scFvs were pre-equilibrated with nM concentrations of competitor peptide BoPrP (96–105) comprising the epitope. The mixtures were then allowed to bind to surface-immobilized antigen and compared to samples containing no competitor. The uninhibited binding signal is a measure for the mean binding activity of a particular pool. We observed a declining binding signal of the pool from round to round to the point that only binding activities similar to background were detectable for pool 3, 4, 6, 7 and 8 (Figure 1(b)). Too high a mutational load thus appeared to destroy the functionality of these pools. Interestingly, further *in vitro* recombination of pool 4 in combination with error-prone PCR and enhanced selection pressure enriched a population with restored binding activity in pool 9. It thus appears that the iterative homologous recombination process performed with repeating DNA-shuffling indeed allowed additive recombination of positive mutations, leading to functional improvement of the pool.

Table 1. Summary of the binding kinetics determined with competition Biacore and Kinetic Exclusion Assay (KinExA)

Antibody species	Competition Biacore (6 °C) K_D (pM)[a]	KinExA (6 °C)		
		K_D (pM)[b]	k_{on} ($M^{-1}s^{-1}$)[c]	k_{off} (s^{-1})[d]
chFab				
P	18.0±2.9	9.0±0.20	8.30±0.25×10^5	7.47 · 10^{-6}
scFv				
P	20.0±1.9	15.5±0.40	4.72±0.06×10^5	7.32×10^{-6}
C1	4.1±1.3	1.2±0.03	1.35±0.01×10^6	1.56×10^{-6}
G9	65.0±29	39.9±0.70	3.26±0.05×10^5	1.30×10^{-5}
XF10	n.d.	16.8±0.30	5.18±0.07×10^5	8.67×10^{-6}

[a] K_D was determined as described by Hanes *et al.*[36] using BoPrP (90–105) peptide as competitor.
[b] K_D was determined from dual-curve equilibrium KinExA titration using BoPrP (90–105) peptide as competitor.
[c] Time-resolved KinExA kinetic experiment (direct method) for k_{on} determination using BoPrP (90–105) peptide as antigen.
[d] k_{off} was calculated as the product of k_{on}×K_D.

Pools 1, 2, 5 and 9 retained binding activity of 54%, 30%, 51% and 23%, respectively, with respect to the P scFv (100%). The fact that pool 5 increased its mean binding activity by 21%, compared to its predecessor pool 2, points out the enrichment of binders in the pool after the diversification step carried out with pool 2 (Figure 1(b)).

The amount of competitor antigen needed to inhibit the binding of the scFvs to surface-immobilized antigen correlates with the mean affinity of binders in the pool.[29] When comparing P scFv with the pools retaining the binding activity, it can be seen that only a small reduction (−3%) of the relative inhibition signal occurs at 10^{-9} M competitor concentration in pool 5, reflecting the need for further off-rate selection rounds with increased selection pressure (Figure 1(c)). Due to the enrichment of binding activity in pool 5 (21% compared to pool 2) and the slight reduction of the inhibition signal, pool 5 was subjected to three additional rounds of off-rate selection.

Screening for binders

After ten days of off-rate selection, the selected scFv fragments were cloned into the vector pAK400, *Escherichia coli* was transformed and single clones were expressed in the periplasm. The periplasmic crude extracts were used for inhibition enzyme-linked immunosorbent assay (ELISA) to investigate binding activity and specificity. Of 184 expressed clones, 74 (40%) showed a positive binding signal over background to surface-immobilized BoPrP (90–105). When comparing the binding signals of the selected scFvs with P scFv, prominent differences were observed, arising from better or worse functional expression of these antibody fragments, in

combination with variable periplasmic extraction efficiency when using this rapid screening assay (Figure 2). Expression and purification of clones representing high and low binding signals in the ELISA confirmed mainly the different functional expression level of the selected scFvs (0.5 mg/l/A_{550} for P scFv, 0.64 mg/l/A_{550} for G9 scFv, 0.045 mg/l/A_{550} for H8 scFv, 0.45 mg/l/A_{550} for C1 scFv and 0.04 mg/l/A_{550} for A7 scFv).

All positive binders could be specifically inhibited with the antigen. The deduction of an affinity ranking based on the relative inhibition signal at various competitor concentrations remained doubtful at this stage due to the undefined oligomeric state of the scFvs and the missing normalization of the amount of functional antibody in the crude extract. Additionally, the inhibition ELISA might not be sensitive enough to discriminate selected binders in the low picomolar affinity range from the initial P scFv.

Sixty promising binders were sequenced for further analysis. On average, 6.5 amino acid residues were mutated per gene in the selected binders. Clusters of similar amino acid mutations could be detected in the V_L and V_H domain, arising from early mutation events amplified with PCR. In general, most of the mutations were distributed all over the framework region of V_L and V_H, only few mutations affected the CDR regions. Only a few mutants accumulated more mutations in the CDR regions than in the framework region of the V_L and V_H domain (e.g. C1 scFv and G9 scFv).

Solution-based affinity determination

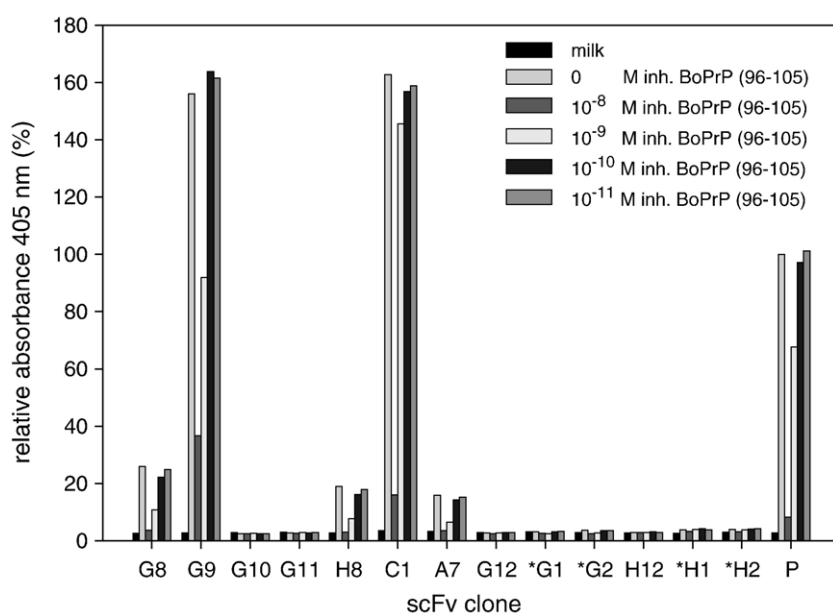A subset of 18 scFv fragments with promising inhibition signals in the ELISA and with similar or

Figure 2. Screening for scFv fragments. Inhibition ELISA with crude extracts of scFvs, expressed in the periplasm of *E. coli*. The crude extracts were preincubated with 0 M to 10^{-11} M of competitor peptide BoPrP (96–105) prior to binding to surface-immobilized antigen and a non-specific control surface. For comparison, the absorbance at 405 nm is depicted as a percentage of the P scFv binding signal. 40% of the investigated clones were active, with binding signals over the background level. The noticeable differences in the binding signal are due to differences in functional expression in combination with variable periplasmic extraction efficiency. The functional expression level (standard shake flask) after purification was determined to 0.64 mg/l/A_{550} for G9 scFv, 0.045 mg/l/A_{550} for H8 scFv, 0.45 mg/l/A_{550} for C1 scFv, 0.04 mg/l/A_{550} for A7 scFv and 0.5 mg/l/A_{550} for P scFv. The detection of the bound scFvs was performed with a mouse anti-His antibody in combination with an alkaline phosphatase-conjugated goat anti-mouse secondary antibody.

better functional expression level than P scFv were chosen for an initial screen of equilibrium dissociation constants (K_D) with competition Biacore,[37,38] using biotinylated BoPrP (90–105) peptide immobilized on a SA-chip. Due to substantial binding of the antibodies to streptavidin on the reference surface, a value that has to be subtracted from the measurements, rather high antibody concentrations in the range of 10 nM to 50 nM had to be chosen to obtain reasonable binding signals over background. Since these antibody concentrations were far above the K_D, only inaccurate affinity determinations were possible, as the complexes are saturated upon titration. The most accurate measurements for equilibrium dissociation constants determination
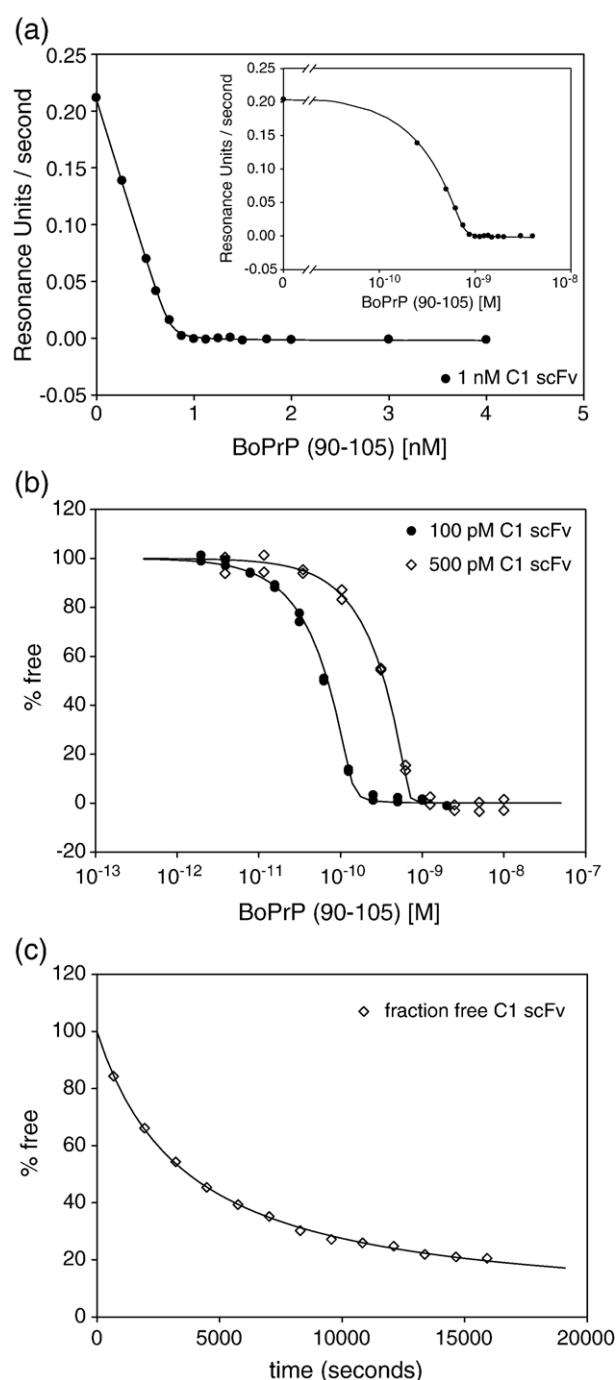
are obtained with antibody concentrations in the range of the K_D. Hence, we were forced to reduce the background binding by investigating other immobilization strategies to allow measurements at low antibody concentrations. We successfully overcame this problem by covalent immobilization of the peptide C-BoPrP (90–111), engineered with an N-terminal cysteine residue, *via* thiol coupling onto the dextran matrix. The most promising antibodies identified in the initial screen were then reinvestigated by competition Biacore (Figure 3(a)). Due to the reduced background binding, the scFv fragment concentrations applied could at least be decreased to 1 nM, but this was still far above the estimated K_D value. For competition, BoPrP (90–105) peptide concentrations from 0.25 nM to 4 nM were applied (Figure 3(a)). The equilibrium dissociation constant for the P scFv was determined as 20 pM. For the affinity-improved clone C1 scFv, we measured a K_D value of 4 pM and for clone G9 scFv, 65 pM (Table 1).

In order to circumvent the use of high antibody concentrations, far above the K_D value necessary in the surface plasmon resonance (SPR) detection method, affinity experiments with KinExA were performed (Figure 3(b) and (c)). One of the great advantages of the KinExA system over the Biacore system for the present experiment is the high sensitivity of the system[39,40] which allows the use of picomolar analyte concentrations, in the range of the K_D in our system, and thus affinities in the low picomolar down to the femtomolar range can be accurately measured. We were able to accomplish equilibrium titration experiments on the KinExA system with antibody concentrations down to 100 pM, which is a factor of 10 below the antibody concentration necessary for competition Biacore measurements.

Azlactone-containing microbeads covalently coupled to the thiol group of C-BoPrP (90–111)

Figure 3. Affinity determination with competition Biacore and KinExA. (a) Competition Biacore binding data of C1 scFv. A 1 nM C1 scFv solution was pre-equilibrated overnight with up to 4 nM of free BoPrP (90–105) peptide prior to injection on a C-BoPrP (90–111) peptide-coated chip. The linear binding rate (r_{obs}), measured under mass transfer limited conditions, is proportional to the concentration of uncomplexed scFv in solution at equilibrium. Each solution was measured in duplicate. The linear binding rate of C1 scFv (slope in RU/s) is plotted as a function of the competitor concentration (filled circles). The corresponding equilibrium dissociation constant K_D was fitted according to Hanes *et al.*[36], which resulted in a $K_D = 4.1$ pM (continuous line). Inset: Logarithmic plot to allow comparison with the KinExA plot in (b). (b) Dual-curve equilibrium KinExA titration of 100 pM (filled circles) and 500 pM (open diamonds) C1 scFv with 1.95 pM–10 nM BoPrP (90–105) peptide concentration. The K_D was fit as 1.2 pM (continuous line). (c) KinExA kinetic experiment using the time resolved method (direct method) for determination the association rate constant k_{on}: equimolar amounts (200 pM) of C1 scFv and peptide were mixed and the fraction of free antibody was traced every 21 min until reaching equilibrium (open diamonds). The association rate constant (k_{on}) was determined as 1.35×10^6 M^{-1}s^{-1} (continuous line).

peptide were used to capture the free portion of the antibody under study, which was equilibrated with different amounts of BoPrP (90–105) peptide. The exposure of the antibody/peptide mixture was sufficiently brief (<500 ms) to ensure negligible dissociation of the complex during the time of exposure to the beads. The scFv fragments captured on the beads were detected with a His tag-specific antibody in conjunction with a secondary fluorescently labeled anti-mouse antibody. The fluorescence signal from the resulting immobilized complex, which is proportional to the quantity of free antibody captured on the beads, was then determined as a fraction of free antibody in solution.

The antibody/BoPrP (90–105) complex was characterized on the KinExA system, performing equilibrium titration measurements over a wide range with BoPrP (90–105) peptide with two constant antibody concentrations. Thereby, K_D-controlled (low concentration, to measure K_D) and antibody-controlled (high concentration, to obtain correct stoichiometry) binding curves were collected and globally fit to achieve a dual-curve analysis (Figure 3 (b)). For the K_D-controlled experiments the antigen concentration was varied in the range of 3 pM to 3 nM (for G9: 20 pM to 20 nM) with an antibody concentration of 100 pM. For the antibody-controlled experiments, the antigen concentration was varied individually for each clone, ranging from between 2 pM and 30 pM at the lower level up to between 5 nM and 50 nM at the upper level, with an antibody concentration of 500 pM (for G9: 2.3 nM). Long incubation times of two days to four days were necessary to reach equilibrium for the K_D-controlled titration. The dual binding curves were globally fit to a 1:1 binding model, resulting in calculated equilibrium dissociation constants of 1.2 pM for the highest affinity clone C1 scFv, 15.5 pM for the original P scFv and 40 pM for the weakest G9 scFv (Table 1).

The association rate constant (k_{on}) was also determined on the KinExA system using the "direct method." In this method, the reduction of free antibody concentration was followed as a function of time as the peptide/antibody reaction approaches equilibrium (Figure 3(c)). Equimolar antibody/ BoPrP (90–105) peptide solutions of 100 pM to 500 pM were followed to equilibrium for a maximum of 8 h. The free antibody fraction was quantified as a function of time after mixing with the antigen. The resulting mono-exponential function was fit to determine k_{on}. The direct kinetic measurement with the highest affinity scFv C1 resulted in a k_{on} value of 1.35×10^6 M^{-1} s^{-1}, and for the original P scFv a k_{on} value of 4.72×10^5 M^{-1} s^{-1} was measured. The dissociation rate constant (k_{off}) for C1 scFv, calculated from the experimentally determined K_D and k_{on} values, was 1.56×10^{-6} s^{-1}; for the original P scFv, k_{off} was calculated as 7.32×10^{-6} s^{-1}.

All the k_{on}, the calculated k_{off} and the K_D values of the antibodies investigated are summarized in Table 1. Note that these measurements all describe the system at 6 °C, where the incubation was carried out. The KinExA system does not have temperature control ability and the samples were chilled prior to and during sampling. With measured affinities in the pM range and the rate constants and concentrations as given above, we do not believe the samples would have time to reestablish a new equilibrium at room temperature during sampling by the KinExA system (maximum exposure time to room temperature would be approximately 40 s).

Structural analysis of P Fab

The crystal structure of the P Fab in complex with the peptide BoPrP (95–104) (sequence: THGQWNKPSK) was determined to a resolution of 2.85 Å.

The CDRs of the heavy (H33–H42, H58–H76, H108–139) and light chain (L25–L42, L58–L72, L107–L139), according to the unified AHo residue numbering scheme[41] used (Figure 4), surround a 14.5 Å deep binding pocket located on the pseudo-2-fold axis relating V_L and V_H (Figure 5). The peptide runs diagonally across the V_L/V_H interface with a distance of 14.3 Å from His P2 to Lys P10. The N-terminal threonine residue of the peptide is not defined in the electron density, which indicates high flexibility of this residue and therefore only poor interaction with the antibody. The C$^\alpha$ of His P2 is located above CDR-L1, its peptide CO accepts a hydrogen bond from the side-chain NH$_2$ of Asn L40, while the C$^\alpha$ of Lys H10 is located above Asp H33 in CDR-H1. The middle of the peptide dips into the deep binding pocket. In particular, the side-chain of Trp P5 inserts deeply into this pocket, while the main-chain CO of P5 accepts a hydrogen bond from the side-chain of His H42. However, the Trp side-chain does not completely fill the pocket (Figure 5). There is room for water molecules between the indole ring of Trp P5 and the side-chains of Arg L54 (CDR-L2), Ile L44 (CDR-L1) and Phe L139 (CDR-L3) that form the V_L-side boundary of the binding pocket. Residues P7 to P10 reside in a groove above CDR-H1, defined by protruding CDR-H2 and CDR-H3 residues. The side-chain ammonium group of Lys P7 donates two hydrogen bonds, one to the side-chain carboxylate of Asp H59, the other to the main-chain CO of Glu H32.

A solvent-accessible surface area of 1400 Å^2 gets buried upon formation of the antibody/peptide complex. The peptide contributes 786 Å^2 of buried surface to the interface, corresponding to 57% of the total solvent-accessible surface area of the peptide. Residue Trp P5 alone contributes 30% of the buried surface of the peptide, followed by residues Lys P7 (17%) and Gln P4 (15%), supporting the observation of a mainly tryptophan-driven antibody/antigen interaction. The heavy and the light chains contribute 64% and 36%, respectively, of buried surface area to the complex. The complex exhibits a high degree of electrostatic and hydrophobic surface complementarity (Figure 6). A cluster of negatively charged side-chains on the V_H domain, consisting of Glu H32, Asp H33 (CDR-

H1), Asp H59, Glu H61, Asp H65 and Glu H67 (CDR-H2) surrounds the positive charges of Lys P7 and Lys P9.

A series of additional specific contacts reinforces the interaction of the peptide with the Fab fragment. The Trp P5 indole nitrogen atom is anchored with the donation of two potential hydrogen bonds (interpreted as a split or alternating H-bond), one to the side-chain carboxylate of Asp H137, the other to the main-chain CO of Arg H108 (Figure 7). The single intramolecular hydrogen bond is donated by the backbone CO of Gly P3 toward the side-chain NH_2 of Gln P4. The positively charged Lys P10 side-chain is directed toward the negatively charged side-chain of Glu H61, which could act as a hydrogen bond acceptor, but with a distance of 3.50 Å, is too remote.

Table 2 delineates the hydrogen bond contacts between the Fab and its epitope. The deep hydrophobic binding pocket is lined by nine aromatic and aliphatic side-chains from both the light and heavy chain: Ile L44, Ile L52, Leu L107, His L109, His H42, Gly H109, Ala H110, Ile H134 and Trp H139. The aromatic plane of His H42 forms a hydrophobic stacking interaction with the indole moiety of Trp P5. A series of further residues of the light and heavy chain flanks the peptide on the surface of the antibody being in van der Waals contact with the peptide: Asp L110, Phe L135, Asp H33, Tyr H40, Tyr-111 and Glu H61.

The peptide itself exhibits a Y-shaped conformation in the complexed structure (Figure 8), allowing Trp P5 to penetrate deep into the hydrophobic cavity. The analysis of the torsion angles in the peptide revealed that this peptide conformation was achieved at the cost of an energetically unfavorable positive Φ torsion angle of residue Gln P4 ($\Phi = 169.33°$, $\Psi = -19.71°$). The binding energy must be big enough to compensate this energy expense required to force the peptide in the binding conformation.

Structural interpretation of C1 antibody mutations

The selected C1 antibody differs from the initial P Fab fragment by a total of six amino acid substitutions (Figures 4 and 5). Four of the six mutations that produce the high affinity binder are located within the CDRs of the antibody; the remaining two residues are framework (FR) mutations: CDR-L1 is affected by the Asn L39Asp mutation and CDR-L2 by the Thr L67Ile mutation; CDR-H2 contains two mutations, namely Glu H67Val and Lys H69Glu; Gly H107Ala is located at the end of FR-3, flanking the CDR-H3 region of the heavy chain and the Arg H47Gly mutation lies in the bottom loop of FR-2.

While analyzing the selected mutations with the use of the wild-type P structure, two mutations, Asn L39Asp and Gly H107Ala, could be identified as being in close proximity to the peptide. These mutations might allow specific ionic and hydrophobic contacts with the peptide, which seem to provide the biggest effect on the affinity improvement observed with the C1 antibody fragment (Figure 8).

Interestingly, the orientation of the original Asn L39 residue (CDR L1) in the P structure exhibits no specific contacts with the peptide. Yet, further analysis of mutation Asn L39Asp, including the adjacent mutation Thr L67Ile, with local energy minimization of a 8 Å sphere around the two mutated residues using the CHARMM27 force field applied to a conjugant gradient minimization algorithm revealed an interesting potential rearrangement of hydrogen bonds with the peptide. Choosing the lowest energy rotamer upon mutating the residue Asn L39 to Asp in the P structure twisted the side-chain by almost 140° ($-77.3°$ to $63.7°$), which brought the residue in closer proximity to the peptide. After minimization, His P2, Asn L39Asp and Asn L40 are turned further toward each other, forming specific interactions (Figure 8(a)): the His P2 side-chain donates a new hydrogen bond of 2.53 Å in length to the Asn L39Asp side-chain oxygen (OD2). The hydrogen bond donated by the Asn L40 side-chain amine to the main-chain CO of His P2 (2.77 Å), already present in the P structure, remained preserved. All the atoms involved in the potential rearranged hydrogen bond interactions of affinity-improved C1 antibody with the peptide are listed in Table 3.

The mutation Thr L67Ile, adjacent in space to Asn L39Asp, probably plays only a tangential role, with a distance of 9.4 Å to the closest atom in the peptide. In the wild-type structure, a hydrogen bond between the main-chain CO of Asn L39 and the side-chain of Thr L67 is lost in the mutant C1. The L67Ile side-chain might add steric bulk, encouraging the flip of Asn L39Asp to interact with and stabilize the position of the His P2 side-chain, which is rather flexible in the wild-type structure (*B*-factor 84.66 Å^2). The influence of the Thr L67Ile mutation in conjunction with Asn L39Asp might therefore be restricted to being a second sphere mutation, possibly supporting the new conformation of Asn L39Asp.

The Glu H67Val and Lys H69Glu mutations in the high affinity C1 antibody fragment lead, on the one hand, to a charge conversion through the substitution of Lys H69 by Glu and, on the other hand, to the destruction of one of the hydrogen bonds connecting to Arg H57 through the presence of the aliphatic Val residue at position H67. In the P structure, residue Arg H57 donates from either of its guanidino NH_2 groups a hydrogen bond to one of the carboxyl oxygen atoms of Glu H67 as well as one to the backbone CO of Glu H67, thereby connecting the two antiparallel β-strands of the CDR-H2 loop. For the V_H type III framework conformation, a structurally important conserved hydrogen bond donated by one of Arg H57 guanidino NH_2 to the main-chain nitrogen atom of Lys H69Glu is not affected.[42] It is very unlikely that the charge conversion induced by Lys H69Glu and a potential slight CDR-H2 rearrangement, observed in a local minimization of a 8 Å sphere around residue H69 including H67 with the
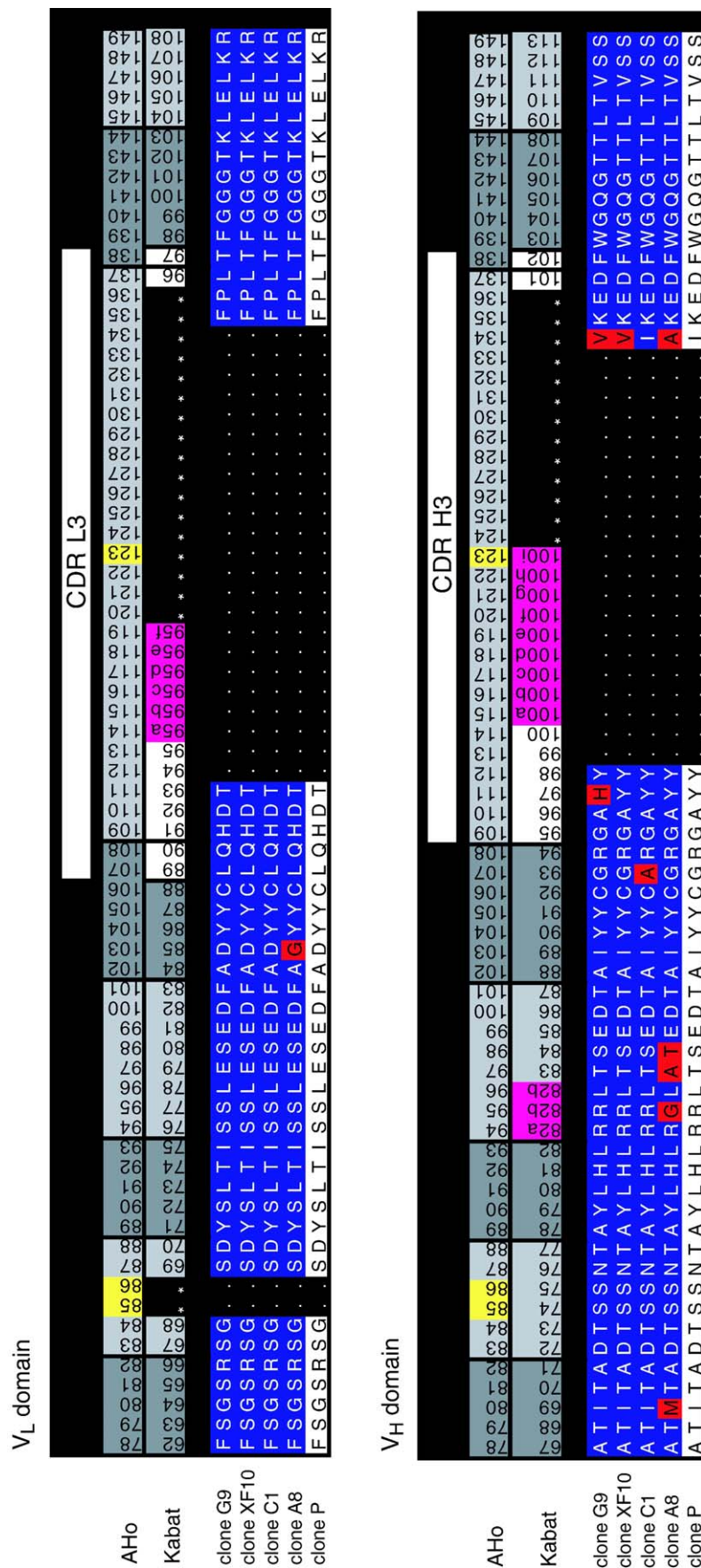
Figure 4 (*legend on next page*)

Figure 4. Sequence alignment of selected scFv fragments. The sequences of the V_L and V_H domain of the selected and characterized scFvs are aligned. AHo[41] and Kabat numbering schemes are depicted for comparison. Numbers with dark gray background represent the structurally most conserved core regions of the domain, whereas those on with light gray background are structurally variable parts. Numbers on pink background indicate the placement of insertions/deletions implied by the Kabat numbering scheme, whereas those on white background designate the position of the CDR regions. The numbers on yellow background marked in the AHo numbering represent the center of sequence alignment gaps placed symmetrically around this position, denoting variable loop length positions in the structure. The accumulated mutations during off-rate selection are highlighted in red. The original P scFv sequence is shown in the last row of the alignment.
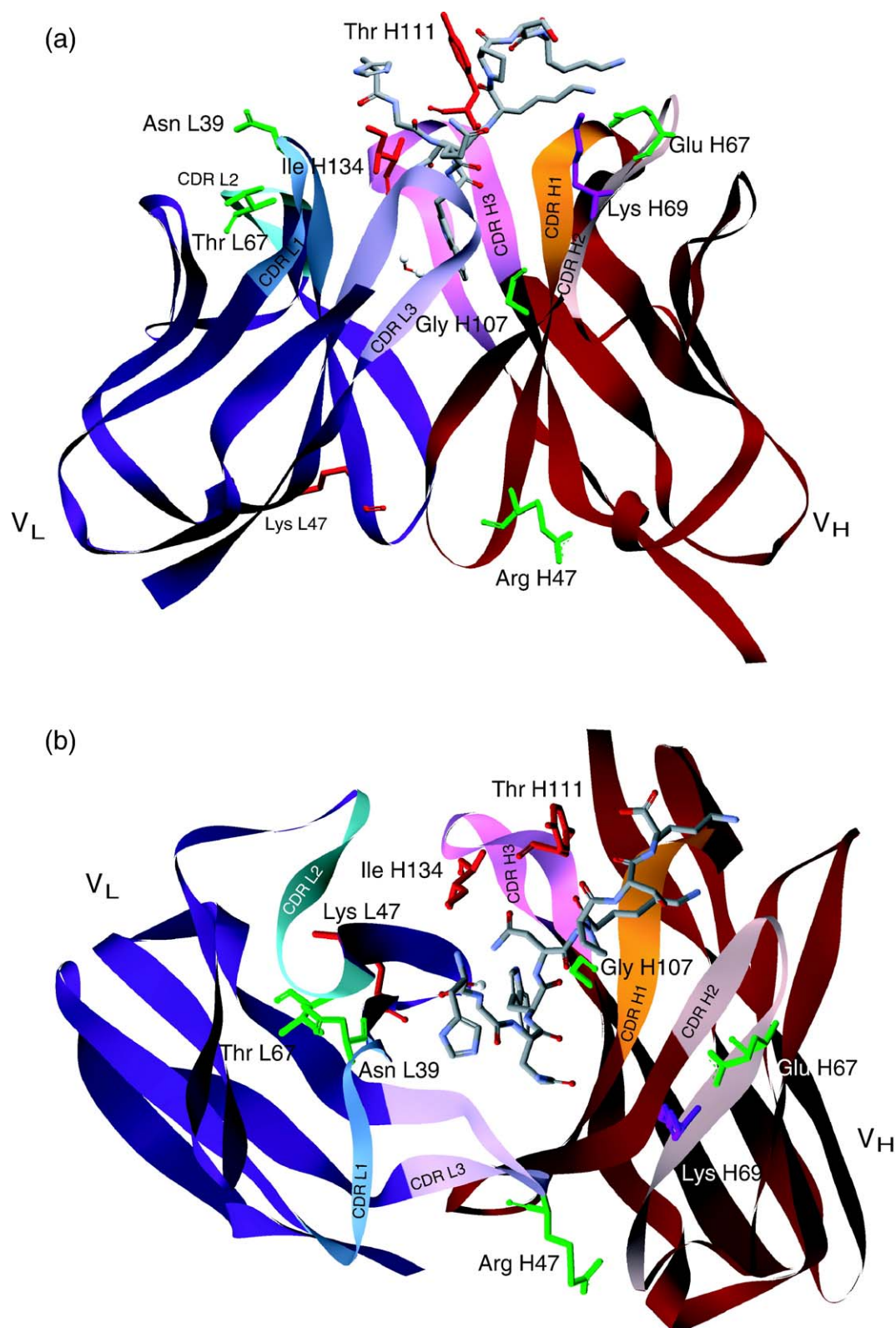
Figure 5. Overall structure of P Fab in complex with the BoPrP (95–104) peptide. (a) Side view and (b) top view. The V_L (dark blue) and V_H (dark red) domain of the P Fab fragment are shown with CDRs colored as follows: CDR-L1, blue; CDR-L2, cyan; CDR-L3, violet; CDR-H1, orange; CDR-H2, light red; CDR-H3, pink. The Y-shaped structure of the BoPrP (95–104) peptide with Trp P5 dipping into the hydrophobic cavity with the presence of a water molecule is illustrated. Residues mutated in antibody C1 are highlighted in green, and residues mutated in antibody G9 are highlighted in red. Residue Lys H69 was mutated in both antibody C1 and G9 and is colored in magenta. Residues are numbered according to AHo numbering scheme (see Figure 4).
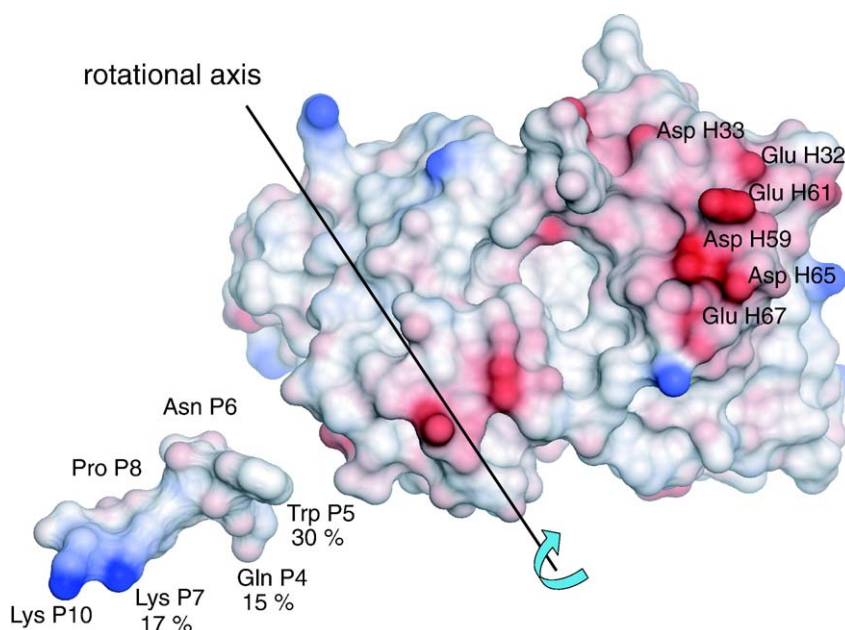
Figure 6. Electrostatic surface potential of the P Fab with the BoPrP (95–104) peptide moved from the binding site. The surface plot illustrates the hydrophobic and electrostatic complementarity of the complex. The positively charged Lys P7 and Lys P10 residues of the peptide complement the negatively charged cluster on the V_H-domain. Trp P5 enters the deep hydrophobic cavity and contributes 30% to the buried surface of the peptide, while Lys P7 (17%) and Gln P4 (15%) also contribute substantially. Rotation about the axis drawn would reconstitute the antibody/peptide complex.

CHARMM27 force field, applied to a conjugant gradient minimization algorithm, is directly responsible for the observed affinity enhancement in the antibody C1.

However, it might be conceivable that the two CDR-H2 mutations have an indirect (second sphere) influence on the conformation of the neighboring Arg H57 side-chain. The Arg H57 side-chain, released by the Glu H67Val mutation, might adopt another conformation, allowing hydrogen bond formation of the guanidino group with the peptide Gln P4 main-chain CO. Thereby, the structurally important conserved hydrogen bond between Arg H57 side-chain and Lys H69Glu main-chain CO for the V_H type III framework conformation[42] would be destroyed. The Lys H69Glu mutation might additionally support the side-chain rearrangement of Arg H57 by providing an alternately oriented ionic interaction with Arg H57. Provided that the loss of the conserved CDR-H2 loop connecting hydrogen bond can structurally be compensated, this would lead to an additional specific hydrogen bond formation with the peptide with a non-mutated residue *via* two second sphere mutations.
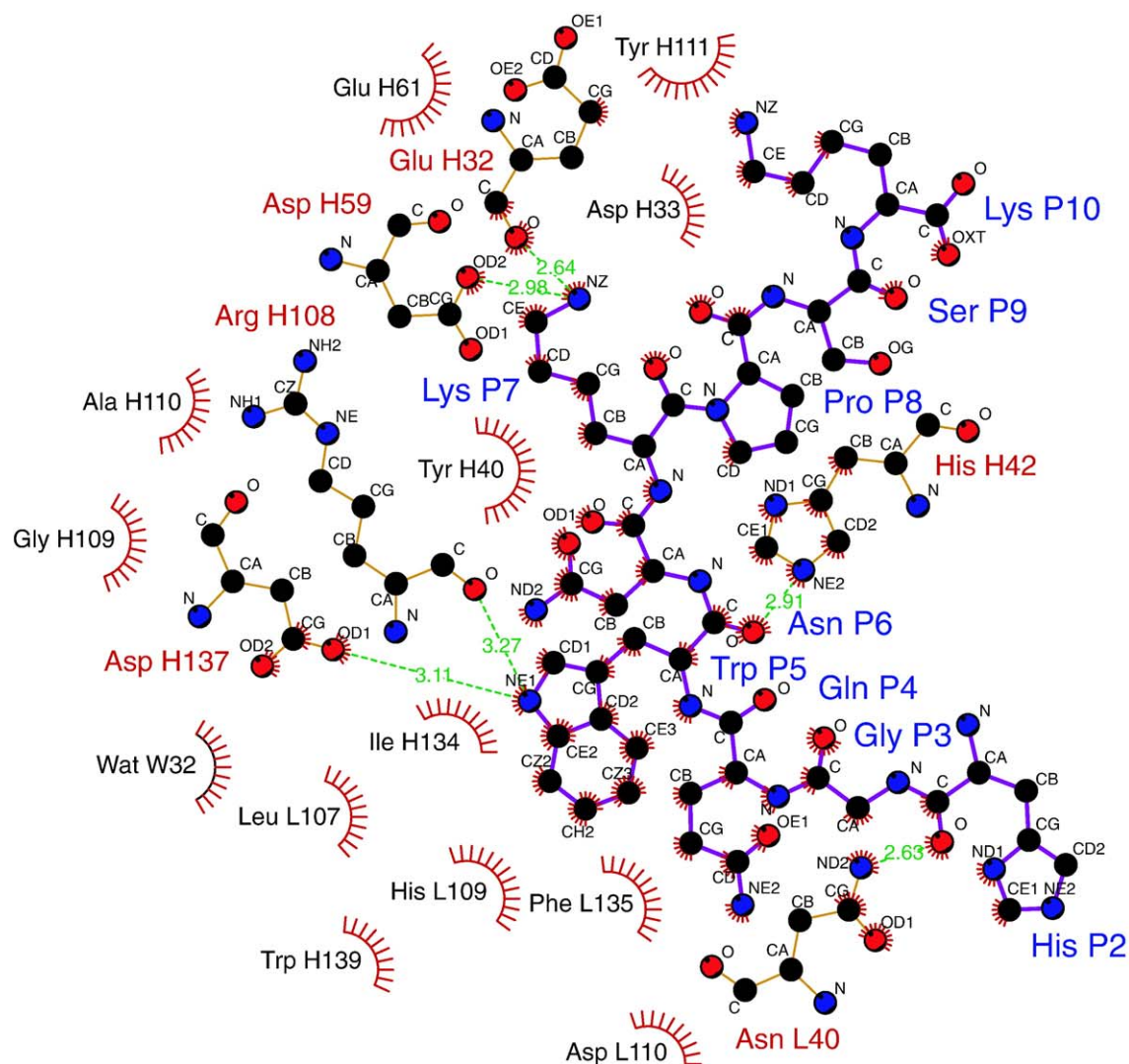
The Gly H107Ala mutation is oriented toward the hydrophobic cavity formed by the heavy and light chain, into which the peptide Trp P5 side-chain binds deeply (Figure 8(b)). The torsion angles of $\Phi = -114.5°$ and $\Psi = 142.4°$ for Gly H107 in the P structure enables a substitution with Ala without major rearrangement of the backbone structure of the following CDR-H3 loop, due to the sterically allowed negative Φ torsion angle for Ala. The methyl group of Ala fits very well into the available space between His H42 and Trp H139 and contributes to the hydrophobic binding interface of the cavity. Since the wild-type cavity is too large for the Trp side-chain and the Ala C^β atom is within 3.4 Å of the $C^{\zeta 2}$ atom of Trp P5, the Gly H107Ala mutation may contribute some van der Waals (VdW) interac-

tion upon peptide binding, which can positively influence the affinity.

The remaining mutation Arg H47Gly on the bottom loop of FR-2 is not in close contact with the peptide. From the sequence analysis of the clones screened in the ELISA experiments, we observed that in 75% of all clones, residue Arg H47 was mutated either to serine (47%) or to glycine (45%). These mutations often occurred in combination with the mutation of residue Glu H49 (in 39% of all analyzed clones), where glutamate was mostly changed to glycine (91%). Early mutation events during error-prone PCR and further propagation of the mutations during the selection lead to their high frequency of appearance. Conceivably, these mutations might positively influence the folding efficiency by supporting the bottom loop formation in the lower core, connecting the CDR-H1 with CDR-H2 with the conformationally more flexible glycine residue and the loop-stabilizing serine residue. This has not been studied in detail, and scFv C1 does not have a dramatically improved expression yield, as the effect of several mutations may cancel each other.

Structural aspects of the low affinity G9 antibody

During the selection, we also isolated an antibody called G9 with three- to fourfold weaker affinity to the peptide than the initial P antibody. The G9 antibody deviates from the P sequence by a total of four mutations, located in CDR-H3 (Tyr H111His, Ile H134Val), CDR-H2 (Lys H69Arg) and FR-2 (Lys L47Arg) (Figures 4 and 5). The identification of one or more mutations responsible for the weaker affinity based on the P structure turned out to be difficult. The antibody G9 carried three mutations in close proximity to the peptide: Tyr H111His, Ile H134Val and Lys H69Arg. In the P structure, both residues Tyr H111 and Ile H134 are in hydrophobic contact with the peptide, either flanking the peptide

Figure 7. LIGPOT of P Fab in complex with BoPrP (95–104) peptide. Detailed hydrogen bonding and hydrophobic contact formation of the peptide with the antibody are depicted in the LIGPLOT.[60] For complementation see also Table 2.

on the surface of the antibody or building the V_H-side boundary of the hydrophobic cavity. As the Lys H69 residue, also mutated to a Glu in the antibody C1, Arg H69 does not directly interact with the peptide. The vicinity and bulkiness of these residues might be the reason for the less than optimal interaction with the peptide in the antibody G9, provided the peptide undergoes no compensating conformational rearrangement. To analyze this

effect, a local energy minimization of a 8 Å sphere around the mutations using the same force field and algorithm as described above was performed, revealing a general rearrangement of peptide residues P6 to P10 and the CDR-H3 loop, including residues Tyr H112 and Ala H110. The following additional specific contacts became possible: Tyr H111His side-chain might donate a 2.65 Å hydrogen bond to the backbone CO of Lys P7 and a 2.56 Å

Table 2. Summary of hydrogen bond interactions of P Fab in complex with BoPrP (95–104) peptide

Peptide atom	P Fab atom	Distance (Å)
His P2 O	Asn L40 ND2	2.63
Trp P5 NE1	Asp H137 OD1	3.11
Trp P5 NE1	Arg H108 O	3.27
Trp P5 O	His H42 NE2	2.91
Lys P7 NZ	Asp H59 OD2	2.98
Lys P7 NZ	Glu H32 O	2.64

hydrogen bond to the carboxylate terminus of the peptide; Lys H69Arg might donate a hydrogen bond to the backbone CO of Gln P4. The fact that the affinity of this antibody was weaker, mainly due to a faster off-rate, allows the conclusion that the mutations might reduce specific short range interactions, due to the bulkiness of the residues and leading to an additional kinetic barrier. The Lys L47Arg mutation, situated at the bottom loop connecting CDR-L1 and CDR-L2, is too far away to influence the affinity in positive or negative ways. It is therefore most probably a neutral mutation.

Discussion

We describe here the successful affinity maturation of the bovine PrP-binding antibody P to a final affinity of 1 pM. By combining error-prone randomization and DNA-shuffling, a library of the P scFv fragment was generated, which was subsequently used for directed evolution by using ribosome display and off-rate selection against the epitope comprising the peptide BoPrP (90–105) (Figure 1(a)). It was not possible to use the BoPrP (90–145) protein fragment or the whole protein during selection, due to the high aggregation tendency of these constructs under ribosome-display conditions. We therefore focused on improving the affinity of P scFv binding the BoPrP (90–105) peptide, as this peptide lies in an unstructured region of PrP and many prion tests use denaturation and/or proteolysis of the sample.

Five rounds of off-rate selection with incubation times up to ten days resulted in the isolation of the affinity-improved scFv termed C1. The sensitivity of the standard inhibition ELISA method turned out to be insufficient for the affinity discrimination of C1 scFv from the others at these very high affinities. Therefore, the screening of affinity-improved scFv fragments had to be performed with SPR technology, using purified monomeric protein. The exact affinity characterization against the BoPrP (90–105) peptide was very challenging, because of its extraordinarily tight binding. It was finally accomplished by two independent solution-based methods: competition binding using the Biacore instrument and the KinExA (Figure 3). Comparison of the selected C1 scFv with the original P scFv revealed a 13-fold affinity improvement. This number represents the factor between the two equilibrium dissociation constants determined with the more sensitive KinExA system, which allows binding measure-

ments to be made at antibody concentrations in the range of the K_D value, as required for accurate determinations. Even though the library was subjected to a strong off-rate selection pressure, not only was the k_{off} reduced fivefold, but also the k_{on} became threefold faster than in the original P scFv (Table 1).

One principal limitation using competition Biacore for very high-affinity binders (low pM range) is the lower sensitivity, compared to the KinExA system. Since the most reliable values for equilibrium dissociation constants are obtained with antibody concentrations in the range of the K_D (as complexed and free antibody should be of a similar magnitude), the lower sensitivity of the instrument restricts the affinity range that can be studied by competition Biacore. A minimal total antibody concentration of 1 nM to 10 nM was required to obtain acceptable signals of binding to immobilized antigen, when the amount of free scFv was determined from following association rate data as a function of inhibiting peptide in solution. This is a factor of 500 to 50 above the measured K_D value. In contrast, for the KinExA equilibrium titration measurements, we were able to reduce the total scFv antibody concentration down to 100 pM, which is only a factor of 6.5 above the K_D value determined with this technology. Even though the KinExA data are giving the more reliable K_D values, the competition Biacore data are still useful for an initial approximation of the equilibrium dissociation constant, as they are more convenient to measure (Table 1).

With the crystal structure of P Fab in complex with the BoPrP (95–104) peptide, we were able to model the C1 antibody mutations and further structurally interpret the affinity improvement. We analyzed all six mutations present in the C1 mutant, of which the Asn L39Asp and the Gly H107Ala mutations seem to provide the most probable effect on the affinity by establishing new specific ionic and hydrophobic interactions with the peptide. The mutations Thr L67Ile, Glu H67Val and Lys H69Glu might have the potential to act as second sphere mutations, positively influencing the affinity of the antibody C1.

The diagonal arrangement of the BoPrP (95–104) peptide across the V_L/V_H interface of the P Fab allows that additional interactions might occur with the CDR-L1 region, if the peptide is elongated at its N terminus, such as the BoPrP (90–105) peptide, which was used for the selection and affinity determination. But the Y-shaped conformation of the peptide and the structurally undefined threonine residue in the crystal structure are clear indications that an N-terminally elongated peptide from residue 94 to 90 would be highly flexible, and additional interactions with the CDR-L1 are very unlikely (Figure 5). Similarly, further addition of residues and amide modification of the carboxyl terminus of the BoPrP (95–104) peptide do not influence the affinity, since the C terminus already reaches the V_H-domain boundary of the antibody.

The P Fab is successfully used in the CDI assay for discrimination between PrP^C and PrP^{Sc}, based on the very different properties of both molecular species.[20]

The CDI assay exploits the fact that the immunoreactivity of PrP^{Sc} is poor when untreated, but greatly enhanced by denaturation, in contrast to PrP^{C}, whose reactivity does not increase upon denaturation. It is believed that the N-terminal, unstructured part of PrP^{C} (residues 90–120) undergoes a major structural rearrangement, contributing to the high β-sheet content in PrP^{Sc}.[8] The poorer interaction of P Fab for PrP^{Sc} indicates that the actual epitope is structurally constrained in the PrP^{Sc} conformer and

partially inaccessible, impeding optimal Y-shaped epitope conformation with a positive Φ angle of Gln98 (P structure Gln P4) for binding, arguing that either fewer interactions are formed with the antibody, or that the local unfolding (to make the epitope accessible) carries an energetic penalty.

The structure-based modeling of the mutations of the G9 variant illustrates how easily point mutations bordering the binding interface negatively influence the affinity and how finely balanced the optimal
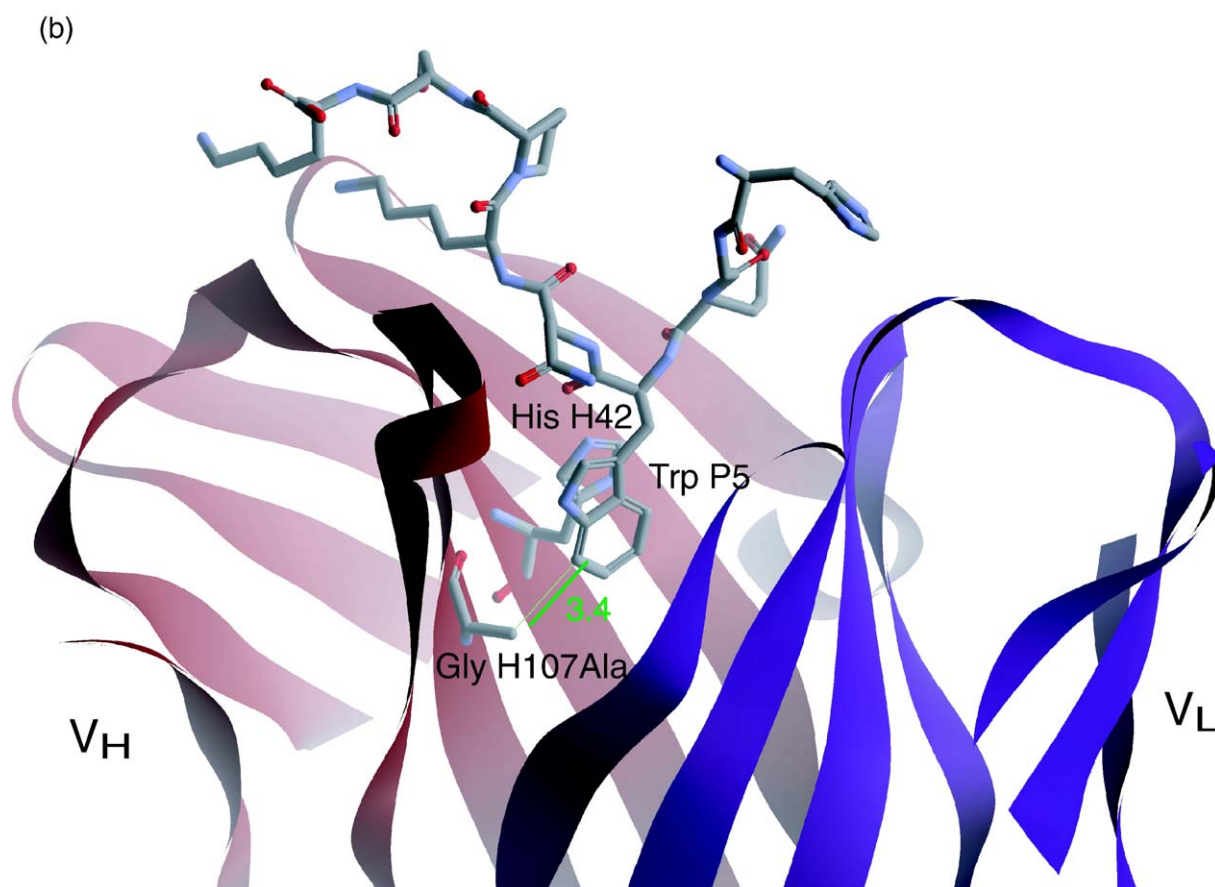

Figure 8 (*legend on next page*)

(b)

Figure 8. Possible new specific interactions of modeled antibody C1 with peptide. (a) Illustration of hydrogen bond formation of modeled antibody C1 with the peptide in a LIGPLOT.[60] His P2 donates a new hydrogen bond to the Asp L39 carboxylate oxygen atom. The original hydrogen bond donated by the Asn L40 side-chain amide to the backbone carbonyl of His P2 is retained. (b) Close-up view of the hydrophobic cavity of the modeled antibody C1, with His H42 forming a stacking interaction with Trp P5 and the mutated Gly H107Ala residue. The V_L and V_H domain are colored in blue and red, respectively. H107Ala fits well into the available space and can contribute VdW interactions, with a distance of 3.4 Å to the closest atom of Trp P5.

interaction is. Deviation of the active antibody concentration could be ruled out as a source for the twofold reduced k_{on} value, as calculations from equilibrium titration experiments with the KinExA instrument allowed a direct determination of the active scFv concentrations.

The originally reported K_D value of P Fab of 0.3 nM–0.5 nM was determined with the PrP protein or the protein fragment, which may also partially

Table 3. Summary of potential hydrogen bond formation of antibody C1 in complex with BoPrP (95–104) peptide

Peptide atom	C1 Fab atom	Distance (Å)
His P2 ND1	Asn L39Asp OD2	2.53 new
His P2 O	Asn L40 ND2	2.77
Trp P5 NE1	Asp H137 OD1	3.11
Trp P5 NE1	Arg H108 O	3.27
Trp P5 O	His H42 NE2	2.91
Lys P7 NZ	Asp H59 OD2	2.98
Lys P7 NZ	Glu H32 O	2.64
C1 Fab atom 1	*C1 Fab atom 2*	*Distance (Å)*
Asn L39Asp OD1	Asn L32 ND2	2.59 new
Asn L39Asp O	Leu L33 N	2.79 new

aggregate. Also, the higher temperature of the measurement (25 °C) may contribute to this difference. While the 13-fold improvement in the affinity of the C1 scFv over that of the original P scFv for bovine PrP could be viewed as rather modest, it should be considered that the original antibody already possessed a K_D value in the mid-picomolar range, indicating that the antibody P had already found a very good structural solution for epitope binding. The complex of the C1 scFv and peptide BoPrP (90–105), with a K_D value of 1.2 pM is the tightest peptide/antibody association ever reported, to the best of our knowledge.

In recent years, extensive efforts were made to develop specific and robust diagnostic tests for bovine, sheep and human prions. Currently, the numerous commercially available diagnostic tests are *post-mortem* assays,[43] measuring PrP^{Sc} in the brain. These tests all use specific antibodies for the detection of the infectious agent PrP^{Sc}, are insufficiently sensitive for *ante-mortem* testing for prions, as the amount of PrP^{Sc} in peripheral tissues, such as blood, during the presymptomatic period is extremely low. Increases in prion diagnostic

sensitivity could result from the concentration or amplification of PrP^{Sc} in test samples and the development of significantly more sensitive detection methods. Newer, recently described assays have focused on these demands.[44] With the protein misfolding cyclic amplification (PMCA) technology, an amplification of small amounts of PrP^{Sc} in biological samples is possible.[45] Immunoassays based on spectroscopic detection techniques such as laser-induced fluorescence spectroscopy using a bead-based sandwich immunoassay,[46] a nanoparticle-based surface-modified fluorescence assay,[47] conformation-dependent immunoassay using time-resolved fluorescence spectroscopy,[11] as well as fluorescence detection after capillary electrophoresis[48] were successfully applied for highly sensitive PrP^{Sc} detection.

When reviewing the commercially available prion diagnostic tests and the newer detection methods described, however, very little is published about the affinities of the antibodies used in these assays. Increasing the affinity of detection antibodies seems to be the most obvious step in lowering the detection limit for essentially all methods and making an existing immunoassay applicable for PrP^{Sc} detection in peripherial tissue.

With the affinity maturation of the C1 scFv to an affinity of 1 pM, we have the key ingredient for a substantially improved diagnostic tool in hand with an increased on-rate and a decreased off-rate for the BoPrP (90–105) peptide. With the slight modification of the common ELISA-based assays, e.g. by presenting the PrP^{Sc} in a more peptide-like conformation through denaturation (as in the CDI[20]) and/or partial digestion, the C1 scFv antibody should improve the sensitivity of the current diagnostic procedures. A combination of PMCA technology with laser-induced fluorescence spectroscopy using the bead-based sandwich immunoassay[46] may be a possible application. Further experiments will be required to examine this antibody in real diagnostic tests.

Materials and Methods

Cloning, expression and purification of antibody fragments

The two variable domains V_L and V_H of the Fab fragment of antibody P[20] were amplified separately from the vector pComb3H-P by using the primers *V$_L$for* (5′-CCATGGACTACAAAGACATCGTGATGACCCA-GACTCCAT-3′) with *V$_L$linker* (5′-GGATCCCGAAGCA-GAACTAGTTTCCGGAGCAGAACTACTGTTGCTCGC-GCCGTTAGGCCGTTTCAGCTCCAGTT-3′) and *V-$_H$linkeradapt* (5′-AGTTCTGCTTCGGGATCCGAGGTG-CAGCTGCTCGAGCA-3′) with *V$_H$gen3SfiI* (5′-AACC-GCCGCCCTCGGCCCCCCGAGGCCGAGGAGACTGT-GAGAGTGGTGCCTT-3′), respectively (linker sequence underlined). With the overlapping non-repetitive linker sequence,[22] both fragments were assembled to the scFv fragment in the orientation V_L-V_H, using primers *V$_L$for* and *V$_H$gen3SfiI*. The P scFv was inserted into the periplasmic expression vector pAK400 between the two unique SfiI restriction sites, thereby introducing a His$_6$ tag at the C terminus.[49]

For construction of the mouse/human chimera Fab (chFab) the variable domains of the antibody P were amplified with the primers *aPV$_L$new* (5′-ATTAC-TCGCGGCCCAGCCGGCCATGGCGGACTACAAA-GATATCGTGATGA CCCAGA-3′) and *V$_L$revMorphBsiWI* (5′-GAGCAGCCACCGTACGTTTTTTCAGCT-CCAGTTTGGTCCC-3′) and with *V$_H$fwdMorphSapI* (5′-TCTTACCGTTGCTCTTCACCCCTGTTAC-CAAAGCCGAGGTGCAGCTGCTCGAGCAGTC-3′) and *V$_H$revMorphSalI* (5′-TGGACCTTTGGTCGACGCTGAGC-TAACCGTCACCAGCGAGGAGACTGTGAGAGTGG-3′). The fragments were subsequently cloned into the periplasmic expression vector pMorphx9_Fab1_kappa_FH with the restriction sites EcoRV/BsiWI for V_L and SapI/SalI for V_H, respectively, generating the mouse/human chimera P Fab fragment (mouseV$_L$κ3-humanC$_L$κ/mouseV$_H$3-humanC$_H$γ1) with a FLAG tag and His$_6$ tag at the C terminus of the heavy chain.

The scFv fragments and the P chFab fragment were expressed in *E. coli* SB536[50] for 6 h and 15 h after 1 mM IPTG induction, respectively, as described.[36] The resuspended cell pellets were lysed with an Emulsiflex apparatus and the crude extract was applied to immobilized metal ion affinity chromatography (Ni^{2+}-NTA, QIAgen) in TBS$_{500}$ (50 mM Tris–HCl (pH 7.4), 500 mM NaCl). After washing with TBS$_{500}$, 5 mM imidazole, 5% (v/v) glycerol, the bound antibody fragments were eluted from the column with TBS$_{500}$, 200 mM imidazole. The partially purified scFvs and P chFab were subsequently subjected to antigen affinity chromatography. For this purpose, N-terminally biotinylated BoPrP (90–105) peptide (GQGGGTHGQW NKPSKP, C-terminal amide; Jerini Peptide Technology (JPT)) had been coupled to a streptavidin-Sepharose matrix (Amersham Biosciences). After being washed with TBS$_{500}$ (pH 7.5), the bound antibody fragments were eluted by using 50 mM glycine (pH 3.0), 150 mM NaCl and immediately neutralized to pH 7–8 with 2 M Tris.

For preparative isolation of the monomeric fraction of scFvs, concentrated samples of 500 μl were applied to a Superdex-200 column (Amersham Biosciences; ÄKTA System) equilibrated with HBS (20 mM Hepes (pH 7.5), 150 mM NaCl) for size exclusion chromatography at 0.5 ml/min. Bovine serum albumin (BSA) (66 kDa), carbonic anhydrase (31 kDa) and cytochrome *c* (12.4 kDa) were used as molecular mass markers. The elution profiles were monitored by absorbance at 280 nm and 230 nm. Fractions of the monomeric peak were collected and combined for further analysis.

Library construction

The P scFv fragment in the vector pAK400 was PCR-amplified using primers *SDAala+* (5′-AGACCACAA-CGGTTTCCCTCTAGAAATAATTTTGTTTAACTTTAA-GAAGGAGATATATCCATGGCGGACTACAAAGAT-3′) and *V$_H$gen3SfiI*. About 1 μg of the PCR product was used for DNA shuffling.[23] Fragments of 100 bp–300 bp in size were generated and reassembled as described.[28] The reassembled DNA served as a template, either for standard PCR amplification in case of library 1, or for further randomization with error-prone PCR in case of library 2; for both PCRs primers, *SDAala+* and *V$_H$gen3SfiI* were used. In total, 18 cycles of error-prone PCR was performed using the dNTP analogs 8-oxo-dGTP and dPTP[24,25] at one-fourth the concentration (25 μM) of each of the dNTPs (100 μM). The final mutation rate of the libraries after DNase I shuffling and error-prone PCR of about 9500 bp was determined by sequencing using standard protocols.

Ribosome display construct

For ribosome display, the 5′ fusion of the T7 promotor and the ribosomal binding site to the library and the in-frame fusion of the gene III spacer sequence were necessary. Instead of assembly PCR, these DNA flanking regions were introduced in every ribosome display round as described,[29] by ligating the PCR fragment *in vitro* to a ribosome display vector very similar to pRDV.[51] The *tolA* gene spacer in pRDV was replaced by the gene III spacer, generating the ribosome display vector pRDVgeneIII. Therefore, the gene III sequence was PCR-amplified with primers *gen3fEcoRI* (5′-GGCCTCGGGGGCCGAATTCGG-CGGTTCTGGTTCCGGTGAT-3′) and *gen3rBglII* (5′-TTAGCAGCCAGATCTTTATCAAGACTCCTTATTACG CAGTATGTTA-3′) from the vector pAK200.[49] The cloning strategy was similar as described,[51] except for the gene III fragment, which was used instead of the *tolA* gene. By simple ligation of the DNA encoding the library into the pRDVgeneIII vector and by a PCR with primers *T7B* (5′-ATACGAAATTAATACGACTCACTATAGGGAGACCA-CAACGG-3′) and *T5te* (5′-CCGCACACCAG TAAGGTG-TGCGGTATCACCAGTAGCACC-3′) using this ligation mix as template, all features necessary for ribosome display were added to the library.

Off-rate selection

The PCR-amplified library was transcribed *in vitro* and subsequently translated for 7 min as described.[36] The ternary complexes of ribosome, mRNA and displayed scFv were equilibrated with 10 nM of biotinylated BoPrP (90–105) peptide at 4 °C overnight. Free BoPrP (90–105) peptide (N-terminal amino group, C-terminal amide; Jerini Peptide Technology (JPT)) was added to a final concentration of 10 μM. The incubation time for competitor exposure in a rollover shaker at 4 °C was increased from round one (10 h) to round five (ten days). The ribosomal complexes were rescued by binding to streptavidin-coated magnetic beads (Roche Applied Science) for 30 min. For removing non-specifically bound complexes, the beads were washed five times for 10 min and the RNA was eluted and purified as described.[36]

Pool analysis with radioimmunoassay (RIA)

For analysis of the scFv pools after the third round of off-rate selection, an inhibition RIA was performed as described.[36] The diluted hot translation mixture was mixed with 1.5 volumes of 4% MPBST (4% (w/v) milk powder in 10 mM Na_2HPO_4 (pH 7.4), 140 mM NaCl, 15 mM KCl, 0.05% (v/v) Tween 20) containing 0 nM, 1.66 nM, 16.6 nM, 166 nM of BoPrP (96–105) peptide (HGQWNKPSKP, N-terminal amino group, C-terminal amide, JPT) and preincubated for 1 h at 4 °C. Binding to biotinylated BoPrP (90–105) peptide (100 μl, 0.25 μM) immobilized on neutravidin-coated microtiter wells (as described)[51] was carried out for 45 min at room temperature (RT). After five washing steps with PBST, the bound radioactive scFv was eluted with 100 μl of 10% (w/v) SDS in PBS and quantified in a scintillation counter.

Inhibition ELISA with crude extract

Two 96-well masterplates were prepared with 100 μl culture (2× YT: 16 g tryptone, 10 g yeast extract, 5 g NaCl per liter, 30 μg/ml chloramphenicol (Cam), 1%(w/v) glucose) of single clones of *E. coli* SB536 cells harboring the selected scFvs in the vector pAK400. They were incubated overnight at 37 °C and subsequently 30% glycerol was added for storage at –80 °C. Two deep well plates with 300 μl of 2× YT/Cam and 0.1% glucose were inoculated with 5 μl of the masterplate cultures. After 2 h of incubation at 28 °C, the cultures were induced for 4 h with 300 μl 2× YT/Cam, containing 1 mM IPTG. Periplasmic extracts were obtained by exposure of the cell pellets to 380 μl of BBS (200 mM boric acid (pH 8.0), 150 mM NaCl, 2 mM EDTA) overnight at 4 °C. The supernatants of the periplasmic extracts were diluted 1:8 with TBST (50 mM Tris–HCl (pH 7.4), 150 mM NaCl, 0.05% Tween 20). These diluted periplasmic extracts were subsequently preincubated with equivalent volumes of 2% MTBST (TBST buffer containing 2% (w/v) milk powder) containing 0 nM, 0.02 nM, 0.2 nM, 2 nM and 20 nM of free BoPrP (96–105) peptide for 1 h at 4 °C. For activity and specificity investigation, these solutions (100 μl/well) were applied for 30 min at RT to biotinylated BoPrP (90–105) peptide immobilized on neutravidin-coated microtiter wells (as described above). After extensive washing with TBST, binding was detected with anti-Tetra-His antibody (QIAgen), and anti-mouse-IgG1-alkaline phosphatase conjugate (Pierce) and *p*-nitrophenylphosphate (Fluka) as substrate. Hydrolysis of the substrate was monitored by measuring the absorbance at 405 nm in a microtiter plate reader (Perkin Elmer).

Affinity determination in solution using competition biosensor technique and KinExA

Biosensor analysis

Competition Biacore measurements were performed on a BIAcore 3000 instrument (BIAcore Inc., Uppsala, Sweden) under mass transport limitation conditions as described.[37,38] On a CM5 chip, the C-BoPrP (90–111) (C-GQGGGTHGQWNKPSKPKTNMKH, N-terminal amino group, C-terminal amide, JPT) peptide (26.8 μM in 10 mM NaOAc (pH 6.0)) was immobilized to up to 700–800 resonance units (RU) using 2-(2-pyridinyldithio)ethaneamine hydrochloride (PDEA) as a coupling reagent. Each binding/regeneration cycle was performed at 25 °C with a constant flow rate of 25 μl/min in HBST (20 mM Hepes (pH 7.5), 150 mM NaCl, 0.005% Tween 20). The purified scFvs (1 nM) were incubated overnight in running buffer with 0.25 nM to 4 nM of BoPrP (90–105) peptide (acting as competitor of binding onto the surface) and the protein was kept at 6 °C prior to injection. In each cycle (6 min), 150 μl of preincubated analyte solution was injected, followed by a 5 μl injection of regeneration solution (3 M NaSCN) and 25 μl injection of running buffer (blank injection) to avoid carry-over of regeneration solution between the reaction cycles. Samples with different competitor concentrations were injected in random order, and every injection was performed twice within each experiment. In order to subtract any background noise from each data set, all samples were also run over an unmodified CM5 dextran surface and random injections of running buffer were performed throughout every experiment for double referencing.[52] The binding data were processed with the software Scrubber (version 1.1f; BioLogic Software, Australia) and further evaluated with BIAevalutaion (BIAcore). The linear slopes of the mass transport-limited binding rate (r_{obs}) were plotted against the competitor concentrations to fit the equilibrium dissociation constant using the equation described earlier.[36]

For the initial screening analysis, where background binding to streptavidin was limiting an accurate affinity determination, the binding data were recorded and processed as described above. The immobilization was based on the streptavidin-biotin interaction: 300 – 600 RU of biotinylated BoPrP (90–105) peptide (50 μg/ml in 10 mM NaOAc (pH 7.5)) were immobilized on a SA-chip (BIAcore). Regeneration was achieved with 25 μl (1 min) injection of 50 mM glycine (pH 2.7).

KinExA analysis

Equilibrium binding studies and measurements of association rate constants were performed using a KinExA 3000 instrument (Sapidyne Instruments Inc, Boise, ID).[53,54] For these experiments, C-BoPrP (90–111) peptide-coated azlactone beads (Sapidyne Instruments Inc, Boise, ID) were used as the capture reagent. The thiol coupling protocol as described above was slightly modified for the immobilization of the peptide to the beads: 18 mg PDEA dissolved in 1 ml carbonate buffer (50 mM Na_2CO_3 (pH 8.5)) was added to 50 mg of azlactone beads and incubated for 1 h at RT while rotating head-over-head. After extensive washing, 150 μg/ml of C-BoPrP (90–111) peptide in 1 ml of carbonate buffer was added to the beads and incubated for 3 h at RT and subsequently overnight at 4 °C. To deactivate the remaining PDEA-SH sites on the previously washed beads, 1 ml of formate buffer (0.1 M HCOONa (pH 4.3), containing 12 mg/ml cysteine and 56 mg/ml NaCl) was added to the beads and incubated for 1 h at RT (head-over-head rotation). The final washing steps of the freshly coated beads prior to use included two rinses with 1 ml and two rinses with 30 ml of HBS buffer (20 mM Hepes (pH 7.4), 150 mM NaCl). The peptide-coated beads were finally stored in 30 ml of HBS buffer (pH 5.3) at 4 °C, to avoid spurious reduction of the S–S bond. During measurements, the beads were collected and subjected to regeneration for repeated usage. The regeneration procedure encompassed two 30 ml washes with 2 M glycine (pH 3.0), two rinses with 30 ml of 30% glycerol and finally two washes with 30 ml of HBS (pH 5.3).

For all equilibrium experiments, free BoPrP (90–105) peptide was twofold serially diluted into BSA/HBS running buffer (1 mg/ml BSA in HBS), containing a constant antibody concentration. For K_D-controlled experiments, the scFv concentrations were 100 pM. The antibody-controlled experiment were performed with constant scFv concentrations of 500 pM (for G9, 2.3 nM). The peptide/antibody complexes, with affinities in the pM range, were then incubated for two to four days at 6 °C to reach equilibrium and kept constantly cooled until immediately prior to injection. The solution flow rate for all experiments was 0.25 ml/min. During K_D-controlled and antibody-controlled experiments, 2 to 3 ml of each peptide/antibody sample was drawn through the flow cell. The captured portion of free scFv antibody fragment on the beads was detected using 0.7 to 0.8 ml (0.25 μg/ml or 0.20 μg/ml) of Tetra-His mouse IgG_1 antibody (an anti-His_4 tag specific antibody; QIAgen) in conjunction with the secondary Cy5™-conjugated goat anti-mouse IgG antibody (1 ml, 1 μg/ml, Jackson ImmunoResearch Laboratories, Inc.). Two replicates of each sample were measured for all equilibrium experiments. The equilibrium titration data were fit to a 1:1 binding model using KinExA software (version 2.4; Sapidyne Intruments Inc.).

For the kinetic measurements, the time-resolved method ("direct method") was used to determine k_{on}.

Thereby, the reduction of the free antibody fraction is followed over time until the equilibrium of the antibody/peptide reaction has been reached. For these measurements, prior to equilibrium 1 to 2 ml of antibody/BoPrP (90–105) peptide solution was drawn through the bead pack for each data point at a flow rate of 0.25 ml/min. The same secondary detection antibodies as used in the equilibrium experiments were applied in the kinetic measurements. The time between data points was 21 min for scFvs. The resulting exponential decrease of captured free antibody as a function of time was fit in the KinExA software to a reversible bimolecular rate equation. The k_{off} was calculated as the product of $k_{on} \times K_D$.

Crystallization

Co-crystallization of P Fab with its cognate peptide epitope was accomplished using hanging drops suspended over 1 ml well solutions. The Fab protein was dialyzed against 10 mM Hepes (pH 7.2). The final protein stock was concentrated to 7 mg/ml. An unmodified peptide corresponding to BoPrP (95–104) (THGQWN-KPSK) was synthesized on an automated peptide synthesizer. The Fab/peptide complex was formed by adding a fivefold molar excess of peptide in buffer to the concentrated Fab and used directly. The drop conditions consisted of 9 μl of protein complex mixed with 1 μl of 1.6 M ammonium sulfate. The well solution contained 0.57% saturated $(NH_4)_2SO_4$, pH adjusted to pH 4.6. Crystal trays were stored at room temperature and large crystals appeared within two weeks.

Data collection

Data were collected (Table 4) at the ALS synchrotron on beamline 8.3.1 using a Quantum 210 detector. A single crystal was used for each data set. The data were integrated and reduced using the MOSFLM package.[55]

Molecular replacement and refinement

The structure described was phased by molecular replacement algorithms as implemented in AMoRe.[56] A polyserine search model for the unliganded Fab was constructed from the structure of the 26–10 Fab/digoxin

Table 4. Data collection and refinement statistics

Data set	P Fab complex
Space group	$P3_121$
Unit cell (Å)	$a = 119.83$, $b = 119.13$, $c = 95.53$
Unit cell (deg.)	$\alpha = \beta = 90.00$, $\gamma = 120.00$
Resolution (Å)/highest shell	2.85/2.85–3.00
Unique reflections/highest shell	18,459/2725
Completeness (%)/highest shell	98.4/99.0
Redundancy/highest shell	2.7/2.7
R_{merge}/highest shell	0.068/0.298
Refinements statistics	
Resolution (Å)	43.40–2.85
R_{work}/R_{free}	0.222/0.282
Atoms	3403
Solvent molecules	69
RMS deviations	
Bonds (Å)	0.007
Angles (deg.)	1.41

complex.[57] The variable and constant Fab domains were searched separately, obviating the need to vary the elbow angle within the search model. Solutions were spatially correlated, CDR regions removed, and the resulting coordinates subjected to rigid body refinement in crystallography and NMR system,[58] treating each of the V_H, C_H1, V_L and C_L regions as separate, rigid domains. The resulting model was then positionally refined in crystallography and NMR system.[58] F_o–F_c maps calculated from these coordinates showed clear side-chain density, which was easily correlated to the sequence. Side-chains were added to the structure in a fairly conservative manner. All glycine and alanine residues in the sequence were substituted immediately. Other side-chains were truncated to alanine unless clear density in the F_o–F_c omit maps indicated the correct side-chain (viewed using O[59]). The model was then subjected to simulated annealing coordinate refinement in crystallography and NMR system. New omit maps were then calculated and additional side-chains placed into the density. In this iterative manner, all side-chains were eventually placed. The progress of refinement was monitored by using the R_{free} criterion, with about 5% of the X-ray data being withheld for this purpose. Water molecules were added after the refinement of the protein model had converged. The water molecules were placed only in relatively spherical omit electron density, and within proper hydrogen bond distance and geometry to protein donor or acceptor atoms. Individual B-factors were then refined. Water molecules whose refined B-factors exceeded 60 Å^2 after refinement were removed. The relevant refinement statistics can be found in Table 2. A Ramachandran plot of the Fab alone shows only one non-Gly or Pro residue in the disallowed region, Asp L30, with 93.6% of the residues being in the most favored and 98.6% in the allowed regions.

Protein Data Bank accession code

Coordinates for the P Fab in complex with its peptide epitope have been deposited in the PDB under accession code 2HH0.

Molecular modeling

The coordinates of the heavy and light chain variable domains of the P Fab in complex with the peptide BoPrP (95–104) served as a template for modeling the mutated residues accumulated in the selected scFv C1 and G9. For choosing the lowest energy rotamer of the mutated residues, local energy minimization was performed in the presence of water as solvent using a conjugant gradient minimization algorithm with the CHARMM27 force field. Energy minimization was performed with the program Insight II (Accelrys Software Inc.).

Acknowledgements

References

1. Collinge, J. (2001). Prion diseases of humans and animals: their causes and molecular basis. *Annu. Rev. Neurosci.* **24**, 519–550.
2. Collinge, J. (2005). Molecular neurology of prion disease. *J. Neurol. Neurosurg. Psychiatry*, **76**, 906–919.
3. Glatzel, M., Stoeck, K., Seeger, H., Luhrs, T. & Aguzzi, A. (2005). Human prion diseases: molecular and clinical aspects. *Arch. Neurol.* **62**, 545–552.
4. Legname, G., Baskakov, I. V., Nguyen, H. O., Riesner, D., Cohen, F. E., DeArmond, S. J. & Prusiner, S. B. (2004). Synthetic mammalian prions. *Science*, **305**, 673–676.
5. Prusiner, S. B. (1998). Prions. *Proc. Natl Acad. Sci. USA*, **95**, 13363–13383.
6. Prusiner, S. B., Scott, M. R., DeArmond, S. J. & Cohen, F. E. (1998). Prion protein biology. *Cell*, **93**, 337–348.
7. Leclerc, E., Peretz, D., Ball, H., Solforosi, L., Legname, G., Safar, J. *et al.* (2003). Conformation of PrP^C on the cell surface as probed by antibodies. *J. Mol. Biol.* **326**, 475–483.
8. Peretz, D., Williamson, R. A., Matsunaga, Y., Serban, H., Pinilla, C., Bastidas, R. B. *et al.* (1997). A conformational transition at the N terminus of the prion protein features in formation of the scrapie isoform. *J. Mol. Biol.* **273**, 614–622.
9. Dumoulin, M. & Dobson, C. M. (2004). Probing the origins, diagnosis and treatment of amyloid diseases using antibodies. *Biochimie*, **86**, 589–600.
10. Paramithiotis, E., Pinard, M., Lawton, T., LaBoissiere, S., Leathers, V. L., Zou, W. Q. *et al.* (2003). A prion protein epitope selective for the pathologically misfolded conformation. *Nature Med.* **9**, 893–899.
11. Safar, J. G., Geschwind, M. D., Deering, C., Didorenko, S., Sattavat, M., Sanchez, H. *et al.* (2005). Diagnosis of human prion disease. *Proc. Natl Acad. Sci. USA*, **102**, 3501–3506.
12. Enari, M., Flechsig, E. & Weissmann, C. (2001). Scrapie prion protein accumulation by scrapie-infected neuroblastoma cells abrogated by exposure to a prion protein antibody. *Proc. Natl Acad. Sci. USA*, **98**, 9295–9299.
13. Peretz, D., Williamson, R. A., Kaneko, K., Vergara, J., Leclerc, E., Schmitt-Ulms, G. *et al.* (2001). Antibodies inhibit prion propagation and clear cell cultures of prion infectivity. *Nature*, **412**, 739–743.
14. Prusiner, S. B., Groth, D., Serban, A., Koehler, R., Foster, D., Torchia, M. *et al.* (1993). Ablation of the prion protein (PrP) gene in mice prevents scrapie and facilitates production of anti-PrP antibodies. *Proc. Natl Acad. Sci. USA*, **90**, 10608–10612.
15. Hanes, J. & Plückthun, A. (1997). *In vitro* selection and evolution of functional proteins by using ribosome display. *Proc. Natl Acad. Sci. USA*, **94**, 4937–4942.
16. Roberts, R. W. & Szostak, J. W. (1997). RNA-peptide fusions for the *in vitro* selection of peptides and proteins. *Proc. Natl Acad. Sci. USA*, **94**, 12297–12302.
17. Dunn, I. S. (1996). Phage display of proteins. *Curr. Opin. Biotechnol.* **7**, 547–553.
18. Scott, M. R., Will, R., Ironside, J., Nguyen, H. O.,

Tremblay, P., DeArmond, S. J. & Prusiner, S. B. (1999). Compelling transgenetic evidence for transmission of bovine spongiform encephalopathy prions to humans. *Proc. Natl Acad. Sci. USA*, **96**, 15137–15142.

19. Llewelyn, C. A., Hewitt, P. E., Knight, R. S., Amar, K., Cousens, S., Mackenzie, J. & Will, R. G. (2004). Possible transmission of variant Creutzfeldt-Jakob disease by blood transfusion. *Lancet*, **363**, 417–421.

20. Safar, J. G., Scott, M., Monaghan, J., Deering, C., Didorenko, S., Vergara, J. *et al.* (2002). Measuring prions causing bovine spongiform encephalopathy or chronic wasting disease by immunoassays and transgenic mice. *Nature Biotechnol.* **20**, 1147–1150.

21. Biffiger, K., Zwald, D., Kaufmann, L., Briner, A., Nayki, I., Purro, M. *et al.* (2002). Validation of a luminescence immunoassay for the detection of PrP^{Sc} in brain homogenate. *J. Virol. Meth.* **101**, 79–84.

22. Hennecke, F., Krebber, C. & Plückthun, A. (1998). Non-repetitive single-chain Fv linkers selected by selectively infective phage (SIP) technology. *Protein Eng.* **11**, 405–410.

23. Stemmer, W. P. (1994). Rapid evolution of a protein in vitro by DNA shuffling. *Nature*, **370**, 389–391.

24. Zaccolo, M. & Gherardi, E. (1999). The effect of high-frequency random mutagenesis on *in vitro* protein evolution: a study on TEM-1 beta-lactamase. *J. Mol. Biol.* **285**, 775–783.

25. Zaccolo, M., Williams, D. M., Brown, D. M. & Gherardi, E. (1996). An approach to random mutagenesis of DNA using mixtures of triphosphate derivatives of nucleoside analogues. *J. Mol. Biol.* **255**, 589–603.

26. Scott, J. K. & Smith, G. P. (1990). Searching for peptide ligands with an epitope library. *Science*, **249**, 386–390.

27. Hawkins, R. E., Russell, S. J. & Winter, G. (1992). Selection of phage antibodies by binding affinity. Mimicking affinity maturation. *J. Mol. Biol.* **226**, 889–896.

28. Jermutus, L., Honegger, A., Schwesinger, F., Hanes, J. & Plückthun, A. (2001). Tailoring *in vitro* evolution for protein affinity or stability. *Proc. Natl Acad. Sci. USA*, **98**, 75–80.

29. Zahnd, C., Spinelli, S., Luginbühl, B., Amstutz, P., Cambillau, C. & Plückthun, A. (2004). Directed in vitro evolution and crystallographic analysis of a peptide-binding single chain antibody fragment (scFv) with low picomolar affinity. *J. Biol. Chem.* **279**, 18870–18877.

30. Janin, J. (1997). The kinetics of protein-protein recognition. *Proteins: Struct. Funct. Genet.* **28**, 153–161.

31. Northrup, S. H. & Erickson, H. P. (1992). Kinetics of protein-protein association explained by Brownian dynamics computer simulation. *Proc. Natl Acad. Sci. USA*, **89**, 3338–3342.

32. Schreiber, G. (2002). Kinetic studies of protein-protein interactions. *Curr. Opin. Struct. Biol.* **12**, 41–47.

33. Zhang, H., Kaneko, K., Nguyen, J. T., Livshits, T. L., Baldwin, M. A., Cohen, F. E. *et al.* (1995). Conformational transitions in peptides containing two putative alpha-helices of the prion protein. *J. Mol. Biol.* **250**, 514–526.

34. Boder, E. T., Midelfort, K. S. & Wittrup, K. D. (2000). Directed evolution of antibody fragments with monovalent femtomolar antigen-binding affinity. *Proc. Natl Acad. Sci. USA*, **97**, 10701–10705.

35. Razai, A., Garcia-Rodriguez, C., Lou, J., Geren, I. N., Forsyth, C. M., Robles, Y. *et al.* (2005). Molecular evolution of antibody affinity for sensitive detection of botulinum neurotoxin type A. *J. Mol. Biol.* **351**, 158–169.

36. Hanes, J., Jermutus, L., Weber-Bornhauser, S., Bosshard, H. R. & Plückthun, A. (1998). Ribosome display efficiently selects and evolves high-affinity antibodies *in vitro* from immune libraries. *Proc. Natl Acad. Sci. USA*, **95**, 14130–14135.

37. Karlsson, R. (1994). Real-time competitive kinetic analysis of interactions between low-molecular-weight ligands in solution and surface-immobilized receptors. *Anal. Biochem.* **221**, 142–151.

38. Nieba, L., Krebber, A. & Plückthun, A. (1996). Competition BIAcore for measuring true affinities: large differences from values determined from binding kinetics. *Anal. Biochem.* **234**, 155–165.

39. Drake, A. W., Myszka, D. G. & Klakamp, S. L. (2004). Characterizing high-affinity antigen/antibody complexes by kinetic- and equilibrium-based methods. *Anal. Biochem.* **328**, 35–43.

40. Rathanaswami, P., Roalstad, S., Roskos, L., Su, Q. J., Lackie, S. & Babcook, J. (2005). Demonstration of an *in vivo* generated sub-picomolar affinity fully human monoclonal antibody to interleukin-8. *Biochem. Biophys. Res. Commun.* **334**, 1004–10013.

41. Honegger, A. & Plückthun, A. (2001). Yet another numbering scheme for immunoglobulin variable domains: an automatic modeling and analysis tool. *J. Mol. Biol.* **309**, 657–670.

42. Honegger, A. & Plückthun, A. (2001). The influence of the buried glutamine or glutamate residue in position 6 on the structure of immunoglobulin variable domains. *J. Mol. Biol.* **309**, 687–699.

43. Kübler, E., Oesch, B. & Raeber, A. J. (2003). Diagnosis of prion diseases. *Br. Med. Bull.* **66**, 267–279.

44. Soto, C. (2004). Diagnosing prion diseases: needs, challenges and hopes. *Nature Rev. Microbiol.* **2**, 809–819.

45. Soto, C., Anderes, L., Suardi, S., Cardone, F., Castilla, J., Frossard, M. J. *et al.* (2005). Pre-symptomatic detection of prions by cyclic amplification of protein misfolding. *FEBS Letters*, **579**, 638–642.

46. Kim, J. I., Wang, C., Kuizon, S., Xu, J., Barengolts, D., Gray, P. C. & Rubenstein, R. (2005). Simple and specific detection of abnormal prion protein by a magnetic bead-based immunoassay coupled with laser-induced fluorescence spectrofluorometry. *J. Neuroimmunol.* **158**, 112–119.

47. Henry, J., Anand, A., Chowdhury, M., Cote, G., Moreira, R. & Good, T. (2004). Development of a nanoparticle-based surface-modified fluorescence assay for the detection of prion proteins. *Anal. Biochem.* **334**, 1–8.

48. Yang, W. C., Yeung, E. S. & Schmerr, M. J. (2005). Detection of prion protein using a capillary electrophoresis-based competitive immunoassay with laser-induced fluorescence detection and cyclodextrin-aided separation. *Electrophoresis*, **26**, 1751–1759.

49. Krebber, A., Bornhauser, S., Burmester, J., Honegger, A., Willuda, J., Bosshard, H. R. & Plückthun, A. (1997). Reliable cloning of functional antibody variable domains from hybridomas and spleen cell repertoires employing a reengineered phage display system. *J. Immunol. Methods*, **201**, 35–55.

50. Bass, S., Gu, Q. & Christen, A. (1996). Multicopy suppressors of prc mutant *Escherichia coli* include two HtrA (DegP) protease homologs (HhoAB), DksA, and a truncated R1pA. *J. Bacteriol.* **178**, 1154–1161.

51. Binz, H. K., Amstutz, P., Kohl, A., Stumpp, M. T., Briand, C., Forrer, P. *et al.* (2004). High-affinity binders selected from designed ankyrin repeat protein libraries. *Nature Biotechnol.* **22**, 575–582.

52. Myszka, D. G. (1999). Improving biosensor analysis. *J. Mol. Recognit.* **12**, 279–284.
53. Blake, D. A., Chakrabarti, P., Khosraviani, M., Hatcher, F. M., Westhoff, C. M., Goebel, P. *et al.* (1996). Metal binding properties of a monoclonal antibody directed toward metal-chelate complexes. *J. Biol. Chem.* **271**, 27677–27685.
54. Blake, R. C., II, Pavlov, A. R. & Blake, D. A. (1999). Automated kinetic exclusion assays to quantify protein binding interactions in homogeneous solution. *Anal. Biochem.* **272**, 123–134.
55. Nyborg, J. & Wonacott, A. J. (1977). In (Arndt, U. W. & Wonacott, A. J., eds), pp. 139–152, North-Holland, Amsterdam.
56. Navara, J. (1994). AMoRe: an automated package for molecular replacement. *Acta Crystallog. sect. A*, **50**, 157–163.
57. Jeffrey, P. D., Strong, R. K., Sieker, L. C., Chang, C. Y., Campbell, R. L., Petsko, G. A. *et al.* (1993). 26-10 Fab-digoxin complex: affinity and specificity due to surface complementarity. *Proc. Natl Acad. Sci. USA*, **90**, 10310–10314.
58. Brünger, A. T., Adams, P. D., Clore, G. M., DeLano, W. L., P., Gros, R.W., Grosse-Kunstleve *et al.* (1998). Crystallography & NMR system: A new software suite for macromolecular structure determination. *Acta Crystallog. sect. D*, **54**, 905–921.
59. Jones, T. A., Zou, J. Y., Cowan, S. W. & Kjeldgaard (1991). Improved methods for building protein models in electron density maps and the location of errors in these models. *Acta Crystallog. sect. A*, **47**, 110–119.
60. Wallace, A. C., Laskowski, R. A. & Thornton, J. M. (1995). LIGPLOT: a program to generate schematic diagrams of protein-ligand interactions. *Protein Eng.* **8**, 127–134.

Edited by I. Wilson